Controlling electron transfer in strong time-dependent fields: theory beyond the Golden Rule approximation

Ludwig Hartmann, Igor Goychuk, Peter Hänggi

Angaben zur Veröffentlichung / Publication details:

Hartmann, Ludwig, Igor Goychuk, and Peter Hänggi. 2000. "Controlling electron transfer in strong time-dependent fields: theory beyond the Golden Rule approximation." *The Journal of Chemical Physics* 113 (24): 11159–75. https://doi.org/10.1063/1.1326049.

The Journal of Chemical Physics

RESEARCH ARTICLE | DECEMBER 22 2000

Controlling electron transfer in strong time-dependent fields: Theory beyond the Golden Rule approximation

Ludwig Hartmann; Igor Goychuk; Peter Hänggi

J. Chem. Phys. 113, 11159–11175 (2000)
https://doi.org/10.1063/1.1326049

AIP Publishing

Controlling electron transfer in strong time-dependent fields: Theory beyond the Golden Rule approximation

Ludwig Hartmann, Igor Goychuk, and Peter Hänggi
Institut für Physik, Universität Augsburg, Universitätsstraße 1, D-86159 Augsburg, Germany

(Received 10 July 2000; accepted 26 September 2000)

In this work we apply a generalized Zusman model to study the influence of an external periodic electric field on the dynamics of electron transfer (ET) reactions coupled to an overdamped reaction coordinate which is treated semiclassically. Being nonperturbative in the tunneling coupling this approach goes beyond the conventional Golden Rule description and includes both adiabatic and nonadiabatic electron transfer regimes. Explicit expressions for the ET rates are derived in the high-frequency driving regime and compared with exact numerical results. Our novel analytical findings constitute a useful approximation scheme, as long as the dynamics can be characterized by a single exponential relaxation. We further demonstrate that the Golden Rule description becomes drastically improved in the presence of strong, fast oscillating fields. Moreover, we discuss interesting phenomena such as an inversion of populations and a driving induced transition from an adiabatic to a nonadiabatic reaction dynamics. © *2000 American Institute of Physics.* [S0021-9606(00)50248-7]

I. INTRODUCTION

The influence of an environment on the reaction rate of electron transfer processes in condensed media presents a long standing problem which still attracts ever growing interest. The current state of the art of the theme of electron transfer is summarized in two recent volumes of *Advances in Chemical Physics*.[1] Especially, the interplay between nonadiabatic and adiabatic electron transfer (ET) regimes is much in the focus of current research activity. Marcus[2] and Hush[3] laid the groundwork to the adiabatic electron transfer theory making use of the *classical* transition state theory (TST) approach. Soon after, Levich and Dogonadze[4] were among the first to address ET as a nonadiabatic process using Fermi's Golden Rule approach. This full quantum-mechanical approach is based on the assumption that the time scale of the fast bath relaxation dynamics and the slow electronic tunneling process can be separated. It corresponds to a relatively small electronic coupling between donor and acceptor sites which is considered perturbatively. In the lowest order of such a perturbation theory the rate of electron transfer is proportional to the square of the electronic coupling. Both adiabatic (strong electronic coupling) and nonadiabatic (weak electronic coupling) approaches to ET have been extended and dwelled upon by many researchers in the field (see, e.g., Ref. 1 for relevant review articles and further references therein).

A promising attempt to unify both wings of the ET theory and to consider the electronic coupling *nonperturbatively* has been undertaken by Zusman[5] and Alexandrov.[6] The original Zusman work envisages the ET reaction as a two-state tunneling problem with a *parabolic* dependence of the electronic energies on the nuclear reaction coordinate. This harmonic reaction coordinate is considered classically; it is assumed to be *overdamped* and because of this fact it can be modeled as a stochastic *Ornstein–Uhlenbeck process*. Zusman then developed a phenomenological theory in replacing the dependence of the electronic levels on the reaction coordinate by the stochastic process in the Hamiltonian making the latter explicitly time-dependent and applying thereafter the Stochastic Liouville Equation approach. Because such approaches yield *incorrect* asymptotic populations, the obtained equations of motion have been corrected ad hoc to ensure the correct thermal detailed balance behavior. Garg, Onuchic, and Ambegaokar[7] provided a full microscopic justification to the phenomenological approach by Zusman[5] and others, and derived Zusman's equations from a time-independent system plus bath Hamiltonian. Their approach opens the doorway how the discussed semiclassical, but *nonperturbative* theory could be generalized further, e.g., including a nonparabolic energy dependence. A special merit of the Zusman approach is the fact that it naturally connects the nonadiabatic and the solvent controlled adiabatic transfer behavior, even though the simplest pictures of the two different regimes of ET reactions appear to be very different from each other.[1]

Several subsequent modifications of the Zusman model have led to the development of more general descriptions. In Refs. 8 and 9, time-dependent solutions of the Zusman model are presented for the case of a polar non-Debye medium with frequency-dependent friction. It was demonstrated that the decay of the donor population becomes strongly nonexponential in contrast to the case of a nonpolar Debye solvent. While most of the previous studies employ essentially two reaction potential surfaces with a one-dimensional reaction coordinate, very recent works concentrate on the generalization of the Zusman approach to electron transfer in three-states systems within a two-dimensional configuration space.[10–12] Within such approaches, problems concerning

multielectron events and/or the interplay between sequential and superexchange mechanisms can be examined.

Recently, the problem of external field control of nonadiabatic ET attracted much attention.[13–17] There, the theory of the driven spin-boson model (see the review[18] for a detailed discussion and further references) has been applied to study periodically *driven* ET dynamics. In those studies, it was shown that in the nonadiabatic Golden Rule regime fast driving can either suppress strongly the rate of electron transfer, or strongly accelerate nonadiabatic ET, as well as to invert the direction of electron transfer.[13,14] Within the present study we shall generalize these previous works beyond the *Golden Rule ET*. In doing so, we shall rely on the conventional, well established quasiclassical formulation of the ET problem by Garg *et al.*,[7] but with the prominent generalization which accounts for time-dependent external driving. Our main objective is to find an answer to the question how external driving fields can influence and control the behavior *beyond the Golden Rule* ET theory. Therefore, our main focus is to generalize the existing concepts[7,19,20] to include the effects of time-dependent driving.

The structure of this paper is as follows. In the next section we briefly review basic concepts in electron transfer theory and introduce our model Hamiltonian. Ideas such as diabatic states, adiabatic states and the Born–Oppenheimer approximation are elucidated. The derivation of the dynamical equations of motion is carried out in Sec. III together with the discussion about their region of validity. There, we shall also introduce the *driven Zusman equations*. Section IV is devoted to the discussion of analytical approaches and corresponding results. In the parameter regime of high-frequency driving we shall show that forward and backward transition rates of the transfer process can be extracted. In Sec. V, we present a numerical formalism to solve the generalized Zusman equations for arbitrary driving forces. Section VI contains a comparison of the numerical findings with the analytical results obtained in Sec. IV. We investigate several effects introduced by the external driving, among those are the inversion of population and the transition from adiabatic to a nonadiabatic electron transfer. Finally, we conclude with a summary of our findings.

II. A GENERALIZED ELECTRON TRANSFER MODEL

An intermolecular electron transfer (ET) reaction is usually associated with a transition between molecular electronic levels which is accompanied by a nuclear rearrangement. To model such processes the relevant electronic states must be known. The foundation of ET theory involves a description in terms of a *localized* electronic initial state, which we will refer to as the *donor* (*D*) or reactant state, and a *localized* final state, which we will refer to as the *acceptor* (*A*) or product state. To determine these *diabatic* molecular states one usually makes use of one of the most prominent concepts in molecular physics and chemistry, the so-called Born–Oppenheimer approximation. In the first stage, the electronic problem is solved while keeping the atomic nuclei (reaction coordinate) fixed in configuration space. In second stage, the nuclear dynamics on a given predetermined potential energy surface is treated. The techniques for calculating

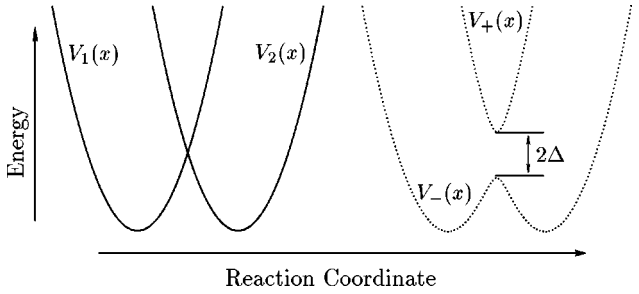

FIG. 1. Schematic representation of two unbiased diabatic Born–Oppenheimer surfaces $V_{1,2}(x)$ and the corresponding adiabatic potentials $V_{\pm}(x)$. The distance between the adiabatic levels is given by twice the nonadiabatic interaction Δ.

these energy surfaces have been developed to a high degree of efficiency in modern quantum chemistry.[21]

A. The model Hamiltonian

The minimal framework to describe driven electron transfer processes consists of two diabatic electronic states $V_{1,2}(x)$ and a generalized one-dimensional reaction coordinate x. The two electronic states before and after the charge transfer are usually denoted as donor $|1\rangle$ and acceptor $|2\rangle$ state, respectively. The reaction coordinate with the effective mass m represents some distinctive nuclear degree of freedom (e.g., a combination of certain intramolecular vibrational modes) coupled to the electronic transfer system.[1] Moreover, the use of the Born–Oppenheimer approximation allows one to formulate the starting Hamiltonian as

$$\hat{H}_{\mathrm{BO}}(x,p,t)=V_1(x,t)|1\rangle\langle 1|+V_2(x,t)|2\rangle\langle 2|+\frac{\hat{p}^2}{2m}. \quad (1)$$

Due to the external driving forces $\mathcal{E}(t)$ the expressions $V_{1,2}(x,t):=V_{1,2}(x)-d_{1,2}\mathcal{E}(t)$ in Eq. (1) are explicitly time dependent. Here, the static diabatic electronic curves $V_{1,2}(x)$ (see Figs. 1 and 2) constitute Born–Oppenheimer potentials for the motion of the reaction coordinate x at the fixed electron configuration $n=1,2$. The influence of the applied elec-

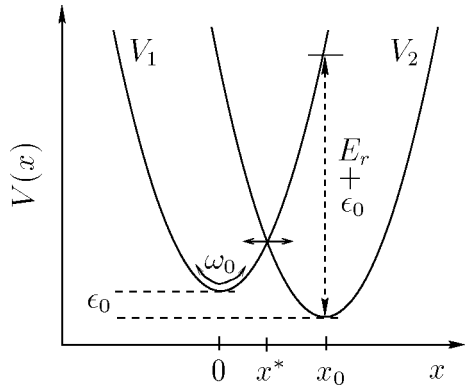

FIG. 2. The diabatic reactant V_1 and product V_2 energy surfaces presented by harmonic functions of the reaction coordinate x [cf. Eq. (5)]. The bias ϵ_0 is the difference between the energy minima of the surfaces. E_r is the reorganization energy, and x^* is the point of intersection at which the electron transfer takes place. The curvature of the wells is characterized by ω_0. The curved arrow indicates relaxation along the reaction coordinate and the straight arrow indicates the crossing motion.

tric field on the electronic subsystem is considered in the dipole approximation, and is given by $d_{1,2}\mathcal{E}(t)$. In this expression $d_{1,2}$ denote the electric dipole moments of the charge density distribution associated with the electron located on the donor or acceptor site, respectively, and $\mathcal{E}(t)$ is the time-dependent field in the semiclassical approximation. Strictly speaking, both $d_{1,2}$ and $\mathcal{E}(t)$ are vectors and their scalar product should be considered. However, we shall assume that the difference of dipole moments is aligned with the electric field and, therefore, we use scalar notations.

Note also that the chosen form of the coupling to the electric field excludes the *direct* influence of the external driving on the reaction coordinate. This assumption means that the reaction coordinate bears only a very small or no associated electric charge or dipole moment. Besides, the dipole moments $d_{1,2}$ generally should depend on the reaction coordinate x. However, we shall neglect this *indirect* influence as a higher order effect, which is beyond the scope of the present work. These very same approximations are implicitly assumed in all previous works on driven electron transfer.[13–15]

To study the influence of external time dependent electric fields on ET processes the Hamiltonian (1) represents the simplest model which can be treated with reasonable efforts. However, the Born–Oppenheimer approximation becomes invalid in the vicinity of the crossing point x^* of the two potential curves where $V_1(x^*)=V_2(x^*)$ (cf. Fig. 2). Here, electronic transitions (tunneling) between the two diabatic electronic levels start to play an important role. This can be accounted for by adding an additional term

$$\hat{H}_{\mathrm{tun}}=\tfrac{1}{2}\Delta(|1\rangle\langle 2|+|2\rangle\langle 1|), \tag{2}$$

to the starting Hamiltonian (1). This contribution is responsible for the coupling between the two surfaces V_1 and V_2. The charge transfer is induced by the electronic coupling matrix element Δ which characterizes the degree of overlap of the donor and acceptor wave function, and which generally also depends on the reaction coordinate. However, we have additionally used the Condon approximation in Eq. (2), assuming that the electronic coupling $\Delta(x):=\Delta$ is a constant.

Moreover, in condensed phase ET complexes, the above system is immersed in a thermal bath which captures the effect of other nuclear and solvent degrees of freedom on the reaction coordinate. Phenomenologically, this situation can be described by friction. On the microscopic level it is modeled by a bilinear coupling of the reaction coordinate to a bath of independent harmonic oscillators of mass m_i and frequencies ω_i. Collecting all our assumptions we end up with the following archetypical Hamiltonian

$$\hat{H}_{\mathrm{ET}}(t)=\tfrac{1}{2}[V_1(x,t)-V_2(x,t)]\hat{\sigma}_z+\tfrac{1}{2}\Delta\hat{\sigma}_x + \frac{1}{2}\left[\frac{\hat{p}^2}{m}+V_1(x,t)+V_2(x,t)\right]\hat{1}+\hat{H}_B, \tag{3}$$

where we have introduced the pseudo-spin operators (Pauli matrices) $\hat{\sigma}_z:=|1\rangle\langle 1|-|2\rangle\langle 2|$, $\hat{\sigma}_x:=|1\rangle\langle 2|+|2\rangle\langle 1|$, and the unity matrix $\hat{1}$, respectively. Furthermore, the term

$$\hat{H}_B=\frac{1}{2}\sum_i\left\{\frac{\hat{p}_i^2}{m_i}+m_i\omega_i^2\left[x_i-\frac{c_i}{m_i\omega_i^2}x\right]^2\right\} \tag{4}$$

in Eq. (3) describes the thermal bath of harmonic oscillators and its coupling to the reaction coordinate. The latter one is written in a separable bilinear form with a so-termed counter term [quadratic in x contribution in Eq. (4)] which removes the renormalization of the potential curves due to friction. This coupling can uniquely be characterized by the bath spectral function $J(\omega)=(\pi/2)\Sigma_i(c_i^2/m_i\omega_i)\delta(\omega-\omega_i)$. In the continuum limit we choose the smooth Ohmic form $J(\omega)=\eta\omega\exp(-\omega/\omega_c)$ with the frequency cutoff $\omega_c\to\infty$ (Ref. 22) and phenomenological friction coefficient η. This constitutes a realistic choice for modeling viscous friction in many ET systems. For example, in experiments with several solvents[23] it has been observed that the behavior of the bath correlation function is qualitatively similar to the theoretical prediction for a solvent with an Ohmic spectral density. Moreover, it is noteworthy that the same Ohmic-type spectral density has been found in simulations of the primary ET in bacterial photosynthesis.[24]

Next, we want to emphasize that the electronic degree of freedom, described by the spin matrices $\hat{\sigma}_{x,z}$, is not directly coupled to the environment. The influence of dissipation on the tunneling dynamics takes place via the reaction coordinate x, which in turn is coupled to the remaining nuclear and solvent degrees of freedom. However, the reaction coordinate in our model is not directly coupled to the external field and experiences the field influence via the electronic degree of freedom only.

B. The potential curves

Basic details of the theory presented below are valid for generic forms of the diabatic potential curves $V_{1,2}(x)$. Nevertheless, we shall restrict ourselves to the standard harmonic oscillator potentials

$$\begin{aligned}V_1(x)&=\tfrac{1}{2}m\omega_0^2x^2,\\ V_2(x)&=\tfrac{1}{2}m\omega_0^2(x-x_0)^2-\epsilon_0,\end{aligned} \tag{5}$$

where x_0 is the spatial displacement between the two shifted parabolic surfaces, and ϵ_0 is the energy distance between the minima. For convenience, the donor well $V_1(x)$ is centered on the coordinate origin. The curvature of the two wells is assumed to be equal and is characterized by ω_0. In the literature the potential curves are often characterized by the well-known reorganization energy

$$E_r=\tfrac{1}{2}m\omega_0^2x_0^2, \tag{6}$$

and the crossing point of the diabatic curves

$$x^*=\frac{x_0}{2}-\frac{\epsilon_0}{m\omega_0^2x_0}=\frac{E_r-\epsilon_0}{2E_r}x_0. \tag{7}$$

We will use these parameters when appropriate. The connection between the various parameters is illustrated with Fig. 2. In the adiabatic basis, the potential energy of the Hamiltonian H_{ET} is diagonalized. The corresponding adiabatic surfaces are the eigenvalues, i.e.,

$$V_{\pm}(x)=\tfrac{1}{2}[V_1(x)+V_2(x)]\pm\tfrac{1}{2}\sqrt{[V_1(x)-V_2(x)]^2+\Delta^2}. \tag{8}$$

If, without driving, the energy gap between the adiabatic surfaces Δ is larger than the thermal energy, $\Delta\gg k_BT$, the upper level is practically not occupied and may be excluded from the further consideration. Thus, an adiabatic description on a single adiabatic surface becomes adequate. When the electronic coupling Δ is relatively small, or time-dependent driving is present, one needs to consider *both* potential surfaces; the reaction can then proceed either adiabatic or nonadiabatic.

III. EQUATIONS OF MOTION

In this section we focus on the derivation of the dynamical equations for the reduced density matrix elements, governed by the electron transfer Hamiltonian $H_{\mathrm{ET}}(t)$ (3). We are particularly interested in a mixed classical-quantum description of the problem, where the reaction coordinate is treated as a classical object moving in a viscous medium and is coupled to the electronic degrees of freedom, which are of a pure quantum nature. The resulting equation of motion for the reduced density operator $\hat{\rho}$ can be derived, e.g., by the cumulant expansion method.[25] Note that the characteristic decay time of correlations in the thermal bath is given (in the limit $\omega_c\to\infty$) by the thermal time $\tau_T=\hbar/(2\pi k_BT)$. If we assume that this time scale is much shorter than any other characteristic time scale of the dynamics of the system (in the absence of dissipation) and the relevant dynamics takes place on the coarse-grained time scale $t\gg\tau_T$, the following Markovian master equation can be derived[7]

$$\frac{d}{dt}\hat{\rho}(t)=-\frac{i}{\hbar}[\hat{H}_{\mathrm{ET}}(t),\hat{\rho}(t)]-\frac{i\eta}{2m\hbar}[\hat{x},[\hat{p},\hat{\rho}(t)]_+]-\frac{\eta k_BT}{\hbar^2}[\hat{x},[\hat{x},\hat{\rho}(t)]], \tag{9}$$

where $[A,B]:=AB-BA$ and $[A,B]_+:=AB+BA$ denote commutator and anticommutator of two arbitrary operators, A and B, respectively. In Eq. (9) the dissipative part has the well-known Caldeira–Leggett form[22] and the region of validity of this equation is given by $k_BT\gg\{\hbar\omega_0,\hbar\eta/m\}$.[25] This means that the reaction coordinate varies on a time scale which is slower as compared to the thermal environment τ_T.

A. Wigner phase-space representation

We are interested in the limit when the quantum behavior of the reaction coordinate and the environment is not important. For this purpose, it will be convenient to represent Eq. (9) in terms of a *quasiprobability* distribution, such as a phase space distribution function. Similar representations have proven to be extremely useful when studying the semiclassical limit of quantum mechanical systems. The most prominent example from a variety of possibilities is given by the Wigner function[26,27]

$$\hat{W}(x,p,t)=\frac{1}{2\pi\hbar}\int_{-\infty}^{+\infty}dx'\,\exp(-ipx'/\hbar)\times\langle x+x'/2|\hat{\rho}(t)|x-x'/2\rangle. \tag{10}$$

Note that $\hat{W}(x,p,t)$ is the 2×2 matrix in the present case. Applying the transformation (10) to the master equation (9) and keeping only terms of leading order in $\hbar(\hbar\to0)$, we end up with the following semiclassical equation of motion,

$$\frac{\partial}{\partial t}\hat{W}(x,p,t)=-\frac{1}{m}\frac{\partial}{\partial x}(\hat{W}p)+\frac{\partial}{\partial p}\left(\hat{W}\frac{d}{dx}\frac{1}{2}[V_1(x,t)+V_2(x,t)]\right)+\frac{\eta}{m}\frac{\partial}{\partial p}(\hat{W}p)+\eta k_BT\frac{\partial^2}{\partial p^2}(\hat{W})+\frac{1}{2}\frac{\partial}{\partial p}[\hat{\sigma}_z,\hat{W}]_+\frac{d}{dx}\frac{1}{2}[V_1(x,t)-V_2(x,t)]-\frac{i}{\hbar}\left[\frac{1}{2}(V_1(x,t)-V_2(x,t))\hat{\sigma}_z+\frac{1}{2}\Delta\hat{\sigma}_x,\hat{W}\right]. \tag{11}$$

We remark that in Eq. (11) the intrinsic quantum mechanical nature of the electron dynamics is depicted by the presence of Planck's constant in the last contribution. The assumption for neglecting higher order terms in $\hbar$ is consistent with the validity regime of Eq. (9). It implies that the relevant energy of the reaction coordinate is small compared to the thermal energy. Therefore, the reaction coordinate can be treated semiclassically. In deriving the Fokker–Planck-type expression (11) we have utilized the operator correspondences

$$\hat{x}\hat{\rho}\leftrightarrow\left(x+\frac{i\hbar}{2}\frac{\partial}{\partial p}\right)\hat{W}(x,p),\quad\hat{\rho}\hat{x}\leftrightarrow\left(x-\frac{i\hbar}{2}\frac{\partial}{\partial p}\right)\hat{W}(x,p), \tag{12}$$

$$\hat{p}\hat{\rho}\leftrightarrow\left(p-\frac{i\hbar}{2}\frac{\partial}{\partial x}\right)\hat{W}(x,p),\quad\hat{\rho}\hat{p}\leftrightarrow\left(p+\frac{i\hbar}{2}\frac{\partial}{\partial x}\right)\hat{W}(x,p).$$

These relations can readily be proved,[28] and for powers of x and p they hold iteratively.

In the next section we shall simplify further the semiclassical equation (11) by assuming the overdamped limit $\gamma\gg\omega_0$ with $\gamma=\eta/m$. In this latter case the reaction coordinate possesses the characteristic relaxation (autocorrelation) time $\tau=\gamma/\omega_0^2$.

B. Zusman equations

In the overdamped limit ($\gamma\gg\omega_0$), the dynamics of the reaction coordinate *momentum* p is not of relevant interest, and thus can be integrated out, i.e., in the basis of localized states, $|i\rangle$, $i=1,2$ we have

$$\rho_{ij}(x,t)=\int_{-\infty}^{+\infty}dp\,W_{ij}(x,p,t), \tag{13}$$

where $(\cdots)_{ij} := \langle i|(\cdots)|j\rangle$. For large times $t \gg \gamma^{-1}$ the equations of motion for $\rho_{ij}(x,t)$ can be obtained by a method termed the inverse friction expansion.[29,30] Here, to leading order in γ^{-1} the distribution for the reaction coordinate momentum p at any space point x is assumed to be Maxwellian so that $\hat{W}$ takes the form

$$W_{ij}(x,p,t) = \frac{1}{\sqrt{2\pi m k_B T}} \exp(-p^2/2mk_BT)\rho_{ij}(x,t). \tag{14}$$

The interested reader can find higher order contributions in the series expansion in Ref. 29. We neglect such complex higher order contributions because they do not provide important corrections as long as the time scale of the driving is long compared to the time scale necessary for the reaction coordinate momentum p to equilibrate.

To ensure the convergence of this method the damping constant has to be sufficiently large. For static harmonic potentials (5) the region of validity is determined by $\gamma \gg \omega_0$.[29]

Bearing all this in mind we finally end up with the novel, semiclassical Smoluchowski-type equations,

$$\begin{aligned}
\frac{\partial}{\partial t}\rho_{11}(x,t) &= \mathcal{L}_1\rho_{11}(x,t) - i\frac{\Delta}{2\hbar}[\rho_{21}(x,t)-\rho_{12}(x,t)],\\
\frac{\partial}{\partial t}\rho_{22}(x,t) &= \mathcal{L}_2\rho_{22}(x,t) - i\frac{\Delta}{2\hbar}[\rho_{12}(x,t)-\rho_{21}(x,t)],\\
\frac{\partial}{\partial t}\rho_{12}(x,t) &= \mathcal{L}\rho_{12}(x,t) - i\frac{\Delta}{2\hbar}[\rho_{22}(x,t)-\rho_{11}(x,t)]\\
&\quad - \frac{i}{\hbar}[V_1(x)-V_2(x)+\epsilon(t)]\rho_{12}(x,t),\\
\frac{\partial}{\partial t}\rho_{21}(x,t) &= \mathcal{L}\rho_{21}(x,t) - i\frac{\Delta}{2\hbar}[\rho_{11}(x,t)-\rho_{22}(x,t)]\\
&\quad + \frac{i}{\hbar}[V_1(x)-V_2(x)+\epsilon(t)]\rho_{21}(x,t).
\end{aligned} \tag{15}$$

Here, the time-dependent electric field influence is contained in the function

$$\epsilon(t) = (d_2 - d_1)\mathcal{E}(t). \tag{16}$$

In Eq. (15) we have defined the two Smoluchowski operators,

$$\begin{aligned}
\mathcal{L}_1 &= D\frac{\partial}{\partial x}\left(\frac{\partial}{\partial x} + \frac{1}{k_BT}\frac{\partial}{\partial x}V_1(x)\right),\\
\mathcal{L}_2 &= D\frac{\partial}{\partial x}\left(\frac{\partial}{\partial x} + \frac{1}{k_BT}\frac{\partial}{\partial x}V_2(x)\right),
\end{aligned} \tag{17}$$

which describe diffusion on the energy surfaces $V_1(x)$ and $V_2(x)$, respectively. Moreover, the operator $\mathcal{L} = (\mathcal{L}_1 + \mathcal{L}_1)/2$ describes diffusion on the averaged potential. The macroscopic diffusion constant D is connected with the phenomenological friction coefficient η and the temperature T by the Einstein relation

$$D = \frac{k_BT}{m\gamma} = \frac{k_BT}{\eta}. \tag{18}$$

The diagonal elements $\rho_{11}(x,t)$ and $\rho_{22}(x,t)$ can be interpreted as the probability distribution functions for the reaction coordinate position x when the electron is situated at the donor or acceptor site, respectively. The external driving force $\epsilon(t)$ in Eq. (15) can be understood as a modulation of the energy gap ϵ_0 between the minima of the two potential surfaces in time. The specific form of this modulation is defined by the time dependence of the driving field $\mathcal{E}(t)$ which can be arbitrary. It is worth noting that, on the phenomenological level of description—using the Smoluchowski like equations (15) instead of the Fokker–Planck equation (11)—corresponds to the assumption that the dynamics of the reaction coordinate can be described by an overdamped oscillator, i.e., inertia effects are neglected. This is a standard assumption met across the literature without much detailed discussion. To determine precisely the region of validity of this assumption requires a separate study which is far beyond the scope of the present work.

In the limit of a vanishing driving amplitude $\epsilon(t) = 0$, Eqs. (15) reduce to those of Garg *et al.*,[7] who obtained them within a path integral scheme. They have also been derived [when $\epsilon(t) = 0$] by Yang and Cukier[19] by a projection operator method. Equations (15) are named in the literature the *Zusman equations*, according to the pioneering work of Zusman,[5] who introduced them in 1980 in a more phenomenological manner using the stochastic Liouville equation approach. One can deduce that our generalized Zusman equations (15) are a hybrid between the equations for the density matrix of spin 1/2 system in an external field and the well-known Smoluchowski equation for diffusion on the two diabatic surfaces $V_1(x)$ and $V_2(x)$.

Recently, the undriven Eqs. (15) have been analytically and numerically investigated by several authors.[7,19,20,31–33] In contrast, we will next focus our attention on the driven, time-dependent case.

IV. ANALYTIC HIGH-FREQUENCY SOLUTION

With Eq. (15) at hand we shall derive an analytic expression for the electron transfer rate constant in the limit of high-frequency driving. To this goal, we shall reduce, by generalizing the reasoning in Ref. 19 onto the driven case, the set of four coupled Zusman equations (15) to only two coupled equations for the diagonal elements $\rho_{11}(x,t)$ and $\rho_{22}(x,t)$.

By formally solving for the two off-diagonal equations for ρ_{12} and ρ_{21} in (15) the diagonal populations are represented by

$$\begin{aligned}
\frac{\partial}{\partial t}\rho_{11}(x,t) &= -\frac{\Delta^2}{2\hbar^2}\mathrm{Re}\int_{-\infty}^{+\infty}dx'\int_0^t dt' G(x,t|x',t')\\
&\quad \times[\rho_{11}(x',t')-\rho_{22}(x',t')] + \mathcal{L}_1\rho_{11}(x,t),\\
\frac{\partial}{\partial t}\rho_{22}(x,t) &= \frac{\Delta^2}{2\hbar^2}\mathrm{Re}\int_{-\infty}^{+\infty}dx'\int_0^t dt' G(x,t|x',t')\\
&\quad \times[\rho_{11}(x',t')-\rho_{22}(x',t')] + \mathcal{L}_2\rho_{22}(x,t),
\end{aligned} \tag{19}$$

where the propagator $G(x,t|x',t')$ is the Green function defined in the operator form by

$$G=[\partial/\partial t-\mathcal{L}+i[V_1(x)-V_2(x)+\epsilon(t)]/\hbar]^{-1}. \tag{20}$$

We explicitly evaluate this Green function in the Appendix for the harmonic surfaces in Eq. (5). The result is given in Eq. (A2) together with Eqs. (A3), (A7), and (A8).

To proceed, we consider a harmonic driving of the form

$$\epsilon(t)=\hat{\epsilon}\cos(\Omega t), \tag{21}$$

and focus our attention on the limit of high-frequency driving, i.e., we assume that the driving period $2\pi/\Omega$ is smaller than any characteristic time of the electron transfer and the diffusive motion in the potential wells. A good approximation to the dynamics of $\rho_{ii}(t)$ then amounts to perform the average of Eq. (19) over a period of the fast driving field to obtain $\overline{\rho}_{ii}(x,t)=\langle\rho_{ii}(x,t)\rangle_\Omega$. The resulting equations for the *averaged* coarse-grained dynamics read

$$\begin{aligned}\frac{\partial}{\partial t}\overline{\rho}_{11}(x,t)&=-\frac{\Delta^2}{2\hbar^2}\mathrm{Re}\int_{-\infty}^{+\infty}dx'\int_0^t dt'\,\overline{G}(x,t-t'|x')\\&\quad\times[\overline{\rho}_{11}(x',t')-\overline{\rho}_{22}(x',t')]+\mathcal{L}_1\overline{\rho}_{11}(x,t),\\\frac{\partial}{\partial t}\overline{\rho}_{22}(x,t)&=\frac{\Delta^2}{2\hbar^2}\mathrm{Re}\int_{-\infty}^{+\infty}dx'\int_0^t dt'\,\overline{G}(x,t-t'|x')\\&\quad\times[\overline{\rho}_{11}(x',t')-\overline{\rho}_{22}(x',t')]+\mathcal{L}_2\overline{\rho}_{22}(x,t),\end{aligned} \tag{22}$$

where $\overline{(\cdots)}:=\langle\cdots\rangle_\Omega$ denotes the time-averaging over the period of the external field. The averaged Green function $\overline{G}(x,t-t'|x')=\langle G(x,t|x',t')\rangle_\Omega$, see Eq. (A2), reads

$$\begin{aligned}\overline{G}(x,t-t'|x')&=G_0(x,t-t'|x')J_0\left(\frac{2\hat{\epsilon}}{\hbar\Omega}\sin\frac{\Omega(t-t')}{2}\right)\\&\quad\times\exp\left[-\frac{i}{\hbar}\epsilon_0(t-t')\right],\end{aligned} \tag{23}$$

with $G_0(x,t-t'|x')$ given in Eq. (A7). To obtain Eqs. (22) and (23) we have used the high-frequency decoupling assumption $\langle G(x,t|x',t')\rho_{ii}(x',t')\rangle_\Omega\approx\overline{G}(x,t|x',t')\overline{\rho}_{ii}(x',t')$ and the well-known relation[13,17,18]

$$\left\langle\exp\left[\frac{i\hat{\epsilon}}{\hbar}\int_{t'}^t\cos(\Omega t'')dt''\right]\right\rangle_\Omega=J_0\left(\frac{2\hat{\epsilon}}{\hbar\Omega}\sin\frac{\Omega(t-t')}{2}\right), \tag{24}$$

where $J_0(z)$ is the zero order Bessel function of the first kind. Hence, for a fast driving field time translation invariance is recovered by this averaging procedure, and the problem becomes formally equivalent to a static one where the influence of the driving has been absorbed in the time dependent prefactor $J_0((2\hat{\epsilon}/\hbar\Omega)\sin[\Omega(t-t')/2])$.

We proceed with performing two further crucial approximations on Eq. (22). First, we assume that the time variation of $G(x,t|x',t')$, which reflects the dynamics of the coherences $\rho_{12}(x,t)$ and $\rho_{21}(x,t)$, is much faster than the dynamics of the populations $\rho_{11}(x',t')$ and $\rho_{22}(x',t')$. Thus, we can apply a Markovian approximation related to the time integral in Eq. (22), yielding

$$\begin{aligned}\frac{\partial}{\partial t}\overline{\rho}_{11}(x,t)&=-\int_{-\infty}^{+\infty}dx'\,M(x|x')[\overline{\rho}_{11}(x',t)-\overline{\rho}_{22}(x',t)]\\&\quad+\mathcal{L}_1\overline{\rho}_{11}(x,t),\end{aligned} \tag{25}$$

with the integral kernel given by

$$M(x|x')=\frac{\Delta^2}{2\hbar^2}\mathrm{Re}\int_0^\infty dt'\,\overline{G}(x,t|x'). \tag{26}$$

By use of the propagator

$$G_{1,2}=(\partial/\partial t-\mathcal{L}_{1,2})^{-1}, \tag{27}$$

describing diffusive motion on the surface $V_{1,2}(x)$, the formal solution of Eq. (25) is given by

$$\begin{aligned}\overline{\rho}_{11}(x,t)&=-\int_{-\infty}^{+\infty}dx''\int_{-\infty}^{+\infty}dx'\int_0^t dt''G_1(x,t''|x'')M(x''|x')\\&\quad\times[\overline{\rho}_{11}(x',t)-\overline{\rho}_{22}(x',t)].\end{aligned} \tag{28}$$

Note, that an analogous equation holds for $\rho_{22}(x,t)$.

In a second step, we follow the Ref. 19 and assuming that the spatial variation of $G_{1,2}(x,t''|x'')$ is much smoother compared to that of $M(x''|x')$ we approximate the integral over x'' in Eq. (28) as $\int dx''G_1(x,t''|x'')M(x''|x')\approx G_1(x,t''|x')\int dx''M(x''|x')$. This approximation is based on the fact that, generally, the diagonal densities in Eq. (15) vary smoothly on the space scale of variations of the off-diagonal densities, see also Refs. 5, 7. Then, by applying G_1^{-1} to the resulting equation we finally obtain

$$\begin{aligned}\frac{\partial}{\partial t}\overline{\rho}_{11}(x,t)&=-K(x)[\overline{\rho}_{11}(x,t)-\overline{\rho}_{22}(x,t)]+\mathcal{L}_1\overline{\rho}_{11}(x,t),\\\frac{\partial}{\partial t}\overline{\rho}_{22}(x,t)&=K(x)[\overline{\rho}_{11}(x,t)-\overline{\rho}_{22}(x,t)]+\mathcal{L}_2\overline{\rho}_{22}(x,t),\end{aligned} \tag{29}$$

where we have introduced the twice-integrated Green function

$$K(x)=\frac{\Delta^2}{2\hbar^2}\mathrm{Re}\int_{-\infty}^{+\infty}dx'\int_0^\infty dt'\,\overline{G}(x',t'|x). \tag{30}$$

Using Eq. (23) and Eqs. (A7)–(A10) in Eq. (30) we obtain

$$\begin{aligned}K(x)&=\frac{\Delta^2}{2\hbar^2}\int_0^\infty dtJ_0\left(\frac{2\hat{\epsilon}}{\hbar\Omega}\sin\frac{\Omega t}{2}\right)\\&\quad\times\cos\left(\frac{E_r\tau}{\hbar}\left(\frac{2x}{x_0}-1\right)(1-e^{-t/\tau})+\frac{\epsilon_0}{\hbar}t\right)\\&\quad\times\exp\left(\frac{2E_rk_BT\tau^2}{\hbar^2}[(1-e^{-t/\tau})\right.\\&\quad\left.+\tfrac{1}{2}(1-e^{-t/\tau})^2-t/\tau]\right).\end{aligned} \tag{31}$$

The integral in Eq. (31) can approximately be evaluated by making a short-time approximation in its integrand. In doing so, the corresponding functions in $\cos(\cdots)$ and $\exp(\cdots)$ in Eq. (31) are expanded to the lowest nonvanishing order in time t, i.e., to the first order in $\cos(\cdots)$ and to the third order in $\exp(\cdots)$. Then, one observes that in the absence of external driving the function $K(x)$ has a peak around the crossing

point of diabatic surfaces x^*, cf. Eq. (7). Moreover, in the presence of driving one finds [using the identity $J_0((2\hat{\epsilon}/\hbar\Omega)\sin(\Omega t/2)) \equiv \Sigma_{n=-\infty}^{\infty} J_n^2(\hat{\epsilon}/\hbar\Omega)\exp(in\Omega t)$ in Eq. (31)] that this peak is splitted into the additional peaks at $\{x_n^* = x^* - n\hbar\Omega x_0/(2E_r),\ n = \pm 1, \pm 2, ...\}$ possessing the relative weights $J_n^2(\hat{\epsilon}/\hbar\Omega)$.

With Eq. (29) we are able to reduce the full Zusman equations (15) to a simpler pair of coupled equations which involve only the populations ρ_{11} and ρ_{22}. The *structure* of Eqs. (29) and (30) is formally equivalent to the expressions obtained in Ref. 19. Therefore, we can follow in our further analysis of Eq. (29) the reasoning therein.

A. Rate equations

Electron transfer processes are characterized by the corresponding transfer rates. In particular, the experimentalists are interested in the rate description (if at all possible) because this provides them with the relevant time scale of the experiment. To extract rate coefficients from Eqs. (29) it is convenient to compare them to some phenomenological rate equations.

1. Phenomenological rate equations

For the generic reaction $DA \rightleftarrows D^+A^-$ the following system of equations is often invoked:

$$\frac{d}{dt}\begin{pmatrix} P_{11}(t) \\ P_{22}(t) \end{pmatrix} = -\begin{pmatrix} k^+ & -k^- \\ -k^+ & k^- \end{pmatrix}\begin{pmatrix} P_{11}(t) \\ P_{22}(t) \end{pmatrix} \equiv -\mathbf{k}\mathbf{P}(t). \tag{32}$$

Here, k^+ and k^- are the rate constants for the forward and backward reaction, respectively, and the corresponding populations $P_{ij}(t)$ on the donor and acceptor surfaces V_1 and V_2, respectively, are obtained by integrating the probability density over configuration space, i.e.,

$$P_{ii}(t) = \int_{-\infty}^{+\infty} dx\, \overline{\rho}_{ii}(x,t). \tag{33}$$

Due to conservation of probability the relation $P_{11}(t) + P_{22}(t) = 1$ holds. With the initial conditions $P_{11}(0) = 1$ and $P_{22}(0) = 0$, Eq. (32) can easily be solved to give

$$P_{11}(t) = P_\infty + (1 - P_\infty)\exp(-\Gamma t). \tag{34}$$

Equation (34) predicts an exponential decay with the total rate constant Γ for the reaction given by the sum of forward and backward rates, i.e.,

$$\Gamma = k^+ + k^-. \tag{35}$$

At long times the stationary limit

$$P_\infty = \frac{k^-}{k^+ + k^-} \tag{36}$$

is reached. Thus, in writing down Eq. (32) we have implicitly made use of the assumption that the relevant dynamics can be described by a single exponential decay. For high-frequency driving, this reasoning is certainly true as long as we are in the overdamped regime and a sufficiently high static barrier exists between the donor and acceptor states. However, the numerical results of Sec. V will prove that even in the activationless regime satisfactory rate results can be obtained.

In terms of the Laplace transformation $\hat{f}(\lambda) = \int_0^\infty \exp(-\lambda t) f(t)$ the population equation (32) reads

$$[\mathbf{k} + \lambda]\hat{\mathbf{P}}(\lambda) = \mathbf{P}(0). \tag{37}$$

2. Derivation of rate equations

An analogous equation can be obtained starting from Eq. (29) with the time independent high-frequency functions $K(x)$, given in Eq. (30). The procedure to achieve this objective is known.[19] We rewrite expression (29) for the diagonal elements of the distribution function in matrix notation, i.e.,

$$\frac{d}{dt}\boldsymbol{\rho}(x,t) = -[\mathbf{K}(\mathbf{x}) - \mathbf{L}]\boldsymbol{\rho}(x,t), \tag{38}$$

with the definitions

$$\boldsymbol{\rho}(x,t) = \begin{pmatrix} \overline{\rho}_{11}(x,t) \\ \overline{\rho}_{22}(x,t) \end{pmatrix}, \quad \mathbf{L} = \begin{pmatrix} \mathcal{L}_1 & 0 \\ 0 & \mathcal{L}_2 \end{pmatrix},$$

$$\mathbf{K}(x) = \begin{pmatrix} K(x) & -K(x) \\ -K(x) & K(x) \end{pmatrix}. \tag{39}$$

Next we perform the Laplace transform on Eq. (38) which results in a similar equation as Eq. (37). However, it still depends on the reaction coordinate x. To achieve an expression for the integrated populations we act on this equation with the projection operator

$$\Pi(\cdots) = \begin{pmatrix} g_1(x) & 0 \\ 0 & g_2(x) \end{pmatrix} \int_{-\infty}^{+\infty} (\cdots)dx = \mathbf{g}(x) \int_{-\infty}^{+\infty} (\cdots)dx,$$
$$g_{1,2}(x) = \frac{\exp(-V_{1,2}(x)/k_BT)}{\int_{-\infty}^{+\infty} dx\, \exp(-V_{1,2}(x)/k_BT)}, \tag{40}$$

and its complement $\mathbf{Q} = \hat{1} - \Pi$. By (i) using standard projection operator manipulations, (ii) utilizing the relations $\Pi\mathbf{L} = 0$, $\mathbf{L}\mathbf{g} = 0$, and (iii) assuming that the initial distributions of the diagonal densities $\overline{\rho}_{ii}(x,0)$ are taken at equilibrium, i.e., $\overline{\rho}_{ii}(x,0) = g_i(x)P_{ii}(0)$, $i = 1,2$, one finds that

$$[\mathbf{m}(\lambda) + \lambda]\hat{\mathbf{P}}(\lambda) = \mathbf{P}(0), \tag{41}$$

with the matrix

$$\mathbf{m}(\lambda) = \mathbf{g}^{-1}\Pi\mathbf{K}(\hat{1} - [\lambda + \mathbf{Q}(\mathbf{K} - \mathbf{L})]^{-1}\mathbf{Q}\mathbf{K})\mathbf{g}. \tag{42}$$

Using some algebraic manipulations and the properties $\mathbf{Q}\mathbf{L} = \mathbf{L}$, $\mathbf{L}\mathbf{g} = 0$, one can identically transform Eq. (42) into the series

$$\mathbf{m}(\lambda) = \mathbf{g}^{-1}\Pi\mathbf{K}\left(\hat{1} - \sum_{n=0}^{\infty} (-1)^n[\tilde{\mathbf{G}}(\lambda)\mathbf{Q}\mathbf{K}]^{n+1}\right)\mathbf{g}, \tag{43}$$

which is convenient to introduce approximations below Eq. (44). In Eq. (43), $\tilde{\mathbf{G}}(\lambda)$ is the diagonal matrix whose elements are the Laplace-transformed Green functions $\tilde{G}_{1,2}(x,\lambda|x') = \int_0^\infty \exp(-\lambda t) G_{1,2}(x,t|x')dt$, where

$G_{1,2}(x,t|x')$ is given in Eq. (A12). Note that $\tilde{G}_{1,2}(x,\lambda|x')$ acts on the arbitrary function $f(x)$ as an integral operator, i.e., $\tilde{G}_{1,2}(\lambda)f := \int_{-\infty}^{\infty}\tilde{G}_{1,2}(x,\lambda|x')f(x')dx'$. Upon comparing Eq. (37) with Eq. (41) we find in the long time limit $t\to\infty$ the identification

$$\mathbf{k} = \lim_{\lambda\to 0}\mathbf{m}(\lambda), \tag{44}$$

for the rate matrix. The evaluation of this equation with Eq. (43) is done in Ref. 19 for the undriven case by means of the so-termed ''consecutive step approximation'' [19] in which the dynamics of diffusion and reaction (tunneling) are disentangled. In our case, we closely follow their evaluation scheme. This consecutive step approximation is in the same spirit as the one used above Eq. (29); it assumes a decoupling between the smooth Green functions in Eq. (43) as compare to the rapidly varying integral kernel $K(x)$ which has a peak around $x=x^*$ [cf. the discussion below Eq. (31)]. In order to obtain a tractable result, we next perform this decoupling consecutively in each term of the series (43).[34] Then, the corresponding series can be summed to yield

$$\mathbf{k} = [\mathbf{1} + \mathbf{K}_{\mathrm{NA}}\mathbf{K}_D]^{-1}\mathbf{K}_{\mathrm{NA}}. \tag{45}$$

Here, the elements of the matrices

$$\mathbf{K}_{\mathrm{NA}} = \begin{pmatrix} k_{\mathrm{NA}}^{+} & -k_{\mathrm{NA}}^{-} \\ -k_{\mathrm{NA}}^{+} & k_{\mathrm{NA}}^{-} \end{pmatrix}, \quad \mathbf{K}_D = \begin{pmatrix} 1/k_D^{+} & 0 \\ 0 & 1/k_D^{-} \end{pmatrix}, \tag{46}$$

are defined via the integral relations

$$k_{\mathrm{NA}}^{\pm} = \int_{-\infty}^{+\infty} dx K(x) g_{1,2}(x), \tag{47}$$

and

$$1/k_D^{\pm} = \int_0^{\infty} dt[\,G_{1,2}(x^*,t|x^*)g_{1,2}(x^*)^{-1} - 1\,]. \tag{48}$$

The explicit expressions for $K(x)$, $g_{1,2}(x)$, and $G_{1,2}(x^*,t|x^*)$ can be found in Eqs. (31), (40), and (A12), respectively.

The rate constants $k_D^{\pm}$ characterize the time scale of diffusion in the two harmonic wells, whereas the crossing dynamics is described by $k_{\mathrm{NA}}^{\pm}$. If the diffusion is rapid relative to the crossing rate, the well population is equilibrated and the standard nonadiabatic (Golden Rule) rate expression is recovered (see Sec. IV B). On the other hand, if the diffusion is slow, it essentially determines the rate of electron transfer rendering the latter essentially independent of the electronic coupling Δ. This can be best seen by writing out the elements of Eq. (45) to obtain the rate expression

$$k^{+} = \frac{k_{\mathrm{NA}}^{+}}{1 + k_{\mathrm{NA}}^{+}/k_D^{+} + k_{\mathrm{NA}}^{-}/k_D^{-}}, \tag{49}$$

which is the usual form for a consecutive step reaction mechanism.[19,35] An analogous equation holds also for the backward rate k^{-} with the interchange $(+\leftrightarrow -)$. In Eq. (49), all the effects of external driving are captured by the field-dependent *nonadiabatic* rate constants $k_{\mathrm{NA}}^{\pm}$. The diffusive rate constants $k_D^{\pm}$ in Eq. (49) are *not* affected by external driving. This clearly reflects a flaw of our approximation scheme when used for the driven case.

It is also interesting to note that a similar rate expression as in Eq. (49) recently emerged in Ref. 15, where *periodically driven* ET was discussed in a rather different system. In this latter work, a model of stochastically gated long range ET has been considered. There, the electron transferring pathway (''bridge'') was stochastically interrupted due to random changes in the conformational configuration of the underlying molecule. Moreover, the conformational dynamics plays there a role similar to the diffusive reaction coordinate in the present work. However, there is a very essential difference between the two models which is reflected in the *different* physical situations considered. In Refs. 15 and 16 the conformational fluctuations *drive* by assumption the ET without any feedback, in the present work the electron transfer dynamics and the reaction coordinate diffusion dynamics are *mutually coupled*. The structure of Eq. (49) indicates however an *effective decoupling* between the diffusion dynamics and the electronic transitions. As a result, the *indirect* influence of external field on the diffusion dynamics is completely disregarded. This decoupling represents thus a drastic approximation which has to be tested against numerical calculations. Notwithstanding these remarks, the approximate result in Eq. (49) motivates us to address such an intriguing effect as the driving-induced transition between the adiabatic and nonadiabatic transfer regime of ET which has been predicted for the conceptually different situation in Refs. 15 and 16.

B. The nonadiabatic rate constant

As will be demonstrated below in Sec. VI B 1, high-frequency and strong driving does actually strongly affect the diffusive rate constants $k_D^{\pm}$, yielding an enhancement that increases with increasing driving strength. Therefore, we may find that $k_D^{\pm} \gg k_{\mathrm{NA}}^{\pm}$, so that the rates $k^{\pm}$ become equal to the nonadiabatic rates $k_{\mathrm{NA}}^{\pm}$ [cf. Eq. (49)]. These rates can be evaluated explicitly. Upon inserting the expressions (31) and $g_{1,2}(x)$ into Eq. (47) and doing the spatial integral analytically, we are led to the very appealing form

$$k_{\mathrm{NA}}^{\pm} = \frac{\Delta^2}{2\hbar^2}\int_0^{\infty} dt J_0\left(\frac{2\hat{\epsilon}}{\hbar\Omega}\sin\frac{\Omega t}{2}\right)\cos\left(\frac{E_r\tau}{\hbar}(1-e^{-t/\tau}) \mp \frac{\epsilon_0}{\hbar}t\right) \times \exp\left(\frac{2E_r k_B T\tau}{\hbar^2}[(1-e^{-t/\tau})\tau - t]\right), \tag{50}$$

where the remaining time integral can be calculated by a numerical quadrature. In deriving this expression we have made use of the Green function (A2) within the high-frequency approximation (23). We want to emphasize that Eq. (50) is one of the central results in this paper. In the absence of driving ($\hat{\epsilon}=0$), it represents nothing but the high-temperature Golden Rule result for the spin-boson model with the Debye spectral density $J_{\mathrm{Debye}}(\omega) = (2E_r/x_0^2)\omega\tau/(1+\omega^2\tau^2)$.[36,37] Thus, our nonadiabatic rate constants (50) present a generalization of the standard Golden Rule results to the case of fast periodic driving. Put differently, by use of

the short-time approximation in (50), i.e., expanding the two terms $(1-e^{-t/\tau})$ in (50) up to the first and second order, respectively, one recovers the previous results in Refs. 13, 14, 18 obtained therein within the short-time and high temperature approximation scheme; see, e.g., Eq. (34) in Ref. 13(a), or Eq. (25) in Ref. 14.

Moreover, the above discussion of Eq. (50) and its derivation based on the Green function (A7) may be understood as an *indirect* proof of our result for the Green function (A7) compared to an incorrect expression given for the undriven case in Ref. 20.

C. The adiabatic rate constant

Also the diffusive rate constants $k_D^{\pm}$ in (48)—which are independent of driving parameters due to made approximations—can be evaluated explicitly. By use of the Green function (A12) and Eq. (40) we obtain

$$1/k_D^{\pm}=\tau\int_0^{\infty}dy\left[\frac{1}{\sqrt{1-e^{-2y}}}\exp\left(\frac{(E_r\mp\epsilon_0)^2}{2E_rk_BT}\,\frac{1}{1+e^{y}}\right)-1\right]. \tag{51}$$

Note that the diffusion rates are inverse proportional to the solvent relaxation time, i.e., $k_D^{\pm}\sim\tau^{-1}=\omega_0^2/\gamma$. Furthermore, the integral in Eq. (51) can be transformed into a more convenient form,

$$1/k_D^{\pm}=\tau\left(\ln(2)+\int_0^1 dz\,\frac{[\exp(E_a^{\pm}z/k_BT)-1]dz}{z\sqrt{1-z}}\right), \tag{52}$$

where $E_a^{\pm}=(E_r\mp\epsilon_0)^2/4E_r$ denote the so-called activation energies. Equation (52) can be expressed in terms of a generalized hypergeometric series ${}_2F_2(a,b;c,d;z)$,[38] to yield

$$\begin{aligned}1/k_D^{\pm}&=\tau\left(\ln(2)+\sum_{n=1}^{\infty}\frac{1}{n(2n-1)!!}\left(\frac{2E_a^{\pm}}{k_BT}\right)^n\right)\\&\equiv\tau\left(\ln(2)+2\left(\frac{E_a^{\pm}}{k_BT}\right){}_2F_2\left(1,1;\frac{3}{2};2;\frac{E_a^{\pm}}{k_BT}\right)\right),\end{aligned} \tag{53}$$

where $(2n-1)!!\equiv 1\cdot 3\cdot 5\cdot\cdots\cdot(2n-1)$. Moreover, for high activation barriers $E_a^{\pm}\gg k_BT$ this result can be well approximated by

$$1/k_D^{\pm}\approx\tau\sqrt{\frac{\pi k_BT}{E_a^{\pm}}}\exp\left(\frac{E_a^{\pm}}{k_BT}\right). \tag{54}$$

Note that in absence of external driving the detailed balance condition,

$$k_{\mathrm{NA}}^{+}/k_{\mathrm{NA}}^{-}=\exp(\epsilon_0/k_BT)=\exp(E_a^{-}/E_a^{+}), \tag{55}$$

holds. Using this and Eq. (54) in the rate expression (49) we obtain in the adiabatic limit $k_{\mathrm{NA}}^{\pm}\gg k_D^{\pm}$ and for $\epsilon_0<E_r$ the forward and backward undriven Kramers rates,

$$\begin{aligned}k^{\pm}\approx k_{\mathrm{ad}}^{\pm}&=\frac{\omega_0^2}{4\gamma}\sqrt{\frac{E_r}{\pi k_BT}}\left[1-\left(\frac{\epsilon_0}{E_r}\right)^2\right]e^{-(E_a^{\pm}/k_BT)}\\&\equiv\frac{\omega_0^2}{\gamma}\sqrt{\frac{E_a^{+}E_a^{-}}{\pi E_rk_BT}}\,e^{-(E_a^{\pm}/k_BT)},\end{aligned} \tag{56}$$

for the activation transitions in the adiabatic potential $V_{-}(x)$, see Eq. (8), and Fig. 1, which is of cusplike form in the limit $\{\Delta,\epsilon_0\}\ll E_r$. Our adiabatic rate expression (56) agrees well with a more general one derived in Ref. 39 for the asymmetric cusp potential. Moreover, for the symmetric case, $\epsilon_0=0$, the original Kramers rate expression[40,41] for the cusp potential is then recovered. Thus, the rate expression (49) reproduces correctly both the nonadiabatic and the adiabatic limit of electron transfer in the *absence* of driving provided that $\Delta\ll E_r$.

With Eqs. (50) and (51) at hand we can next verify our analytical results versus precise numerics.

V. NUMERICAL SOLUTION OF THE DRIVEN ZUSMAN MODEL

First we like to discuss a numerical method for solving the externally driven Zusman equations (15). A very successful scheme that works in absence of a detailed balance relationship (which is broken in a time-dependent driven case) has been proposed by Yang and Cukier.[19] We therefore adopt their numerical scheme for our purpose. In doing so we introduce in place of Eq. (15) the four combinations,

$$\begin{aligned}&\rho^{\pm}=\rho_{11}\pm\rho_{22},\quad 2\,\mathrm{Re}\,\rho_{12}=\rho_{12}+\rho_{21},\\&2\,\mathrm{Im}\,\rho_{12}=\rho_{12}-\rho_{21}.\end{aligned} \tag{57}$$

It is advantageous to work with dimensionless quantities. To this end we introduce a dimensionless time $\tilde{t}=t/\tau$, with the relaxation time of the overdamped harmonic oscillator $\tau=\gamma/\omega_0^2$. Thus the phenomenological time constant in the Zusman model is τ, which is frequently identified with the longitudinal dielectric relaxation time or the average solvation time.[5,31,35,42] Moreover, a dimensionless coordinate $\tilde{x}=\sqrt{m\omega_0^2/k_BT}x$ is defined, where $\sqrt{k_BT/m\omega_0^2}$ is the average width of the oscillator potential surfaces. Using these definitions together with Eqs. (5) and (17) in Eq. (15) we obtain

$$\begin{aligned}\frac{\partial}{\partial\tilde{t}}\rho^{+}(\tilde{t},\tilde{x})&=\tilde{\mathcal{L}}\rho^{+}(\tilde{t},\tilde{x})+\frac{1}{2}\tilde{x}_0\frac{\partial}{\partial\tilde{x}}\rho^{-}(\hat{t},\tilde{x}),\\\frac{\partial}{\partial\tilde{t}}\rho^{-}(\tilde{t},\tilde{x})&=\tilde{\mathcal{L}}\rho^{-}(\tilde{t},\tilde{x})+\frac{1}{2}\tilde{x}_0\frac{\partial}{\partial\tilde{x}}\rho^{+}(\tilde{t},\tilde{x})-\tilde{c}\,\mathrm{Im}\,\rho_{12}(\tilde{t},\tilde{x}),\\\frac{\partial}{\partial\tilde{t}}\mathrm{Re}\,\rho_{12}(\tilde{t},\tilde{x})&=\tilde{\mathcal{L}}\,\mathrm{Re}\,\rho_{12}(\tilde{t},\tilde{x})+\tilde{d}(\tilde{x}-\tilde{x}^{*}(t))\mathrm{Im}\,\rho_{12}(\tilde{t},\tilde{x}),\\\frac{\partial}{\partial\tilde{t}}\mathrm{Im}\,\rho_{12}(\tilde{t},\tilde{x})&=\tilde{\mathcal{L}}\,\mathrm{Im}\,\rho_{12}(\tilde{t},\tilde{x})-\tilde{d}(\tilde{x}-\tilde{x}^{*}(t))\mathrm{Re}\,\rho_{12}(\tilde{t},\tilde{x})\\&\quad+\frac{\tilde{c}}{4}\rho^{-}(\tilde{t},\tilde{x}),\end{aligned} \tag{58}$$

where

$$\tilde{\mathcal{L}}=\left[\frac{\partial^2}{\partial\tilde{x}^2}+\left(\tilde{x}-\frac{1}{2}\tilde{x}_0\right)\frac{\partial}{\partial\tilde{x}}+1\right]. \tag{59}$$

The new dimensionless auxiliary parameters appearing in Eq. (58) are $\tilde{c}=2\tau\Delta/\hbar$ and $\tilde{d}=\sqrt{2E_r k_B T/\hbar\tau}$. The time-dependent crossing point and the spatial displacement read

$$\tilde{x}^*(t)=\frac{E_r-\epsilon_0-\epsilon(t)}{\sqrt{2E_r k_B T}},\quad \tilde{x}_0=\sqrt{2E_r/k_B T}, \tag{60}$$

respectively. In the following we suppress the tildes indicating dimensionless coordinates since there is no risk for confusion. Furthermore, we construct a solution for Eq. (58) by the use of an eigenfunction expansion method. For this purpose we choose as basis functions the right eigenfunctions $r_n(x)$ of the diffusion operator,

$$\tilde{\mathcal{L}} r_n(x)=\mu_n r_n(x), \tag{61}$$

with eigenvalues $\mu_n=-n$, $n=0,1,2,\ldots$. The function $r_n(x)$ is proportional to Hermite polynomial H_n of order n,

$$r_n(x)=\frac{(1/2\pi)^{1/4}}{\sqrt{2^n n!}}H_n[(x-x_0/2)/\sqrt{2}] \times\exp[-(x-x_0/2)^2/2]. \tag{62}$$

Because the right eigenfunctions $r_n(x)$ form together with the left eigenfunctions (which are the right eigenfunctions of the *adjoint* operator),

$$l_n(x)=\frac{(1/2\pi)^{1/4}}{\sqrt{2^n n!}}H_n((x-x_0/2)/\sqrt{2}) =\exp((x-x_0/2)^2/2)r_n(x), \tag{63}$$

a complete set, we can expand the solutions of Eq. (58) as

$$\rho^{\pm}(t,x)=\sum_{n=0}^{\infty} a_n^{\pm}(t)r_n(x),$$

$$\mathrm{Re}\,\rho_{12}(t,x)=\sum_{n=0}^{\infty} b_n^{+}(t)r_n(x), \tag{64}$$

$$\mathrm{Im}\,\rho_{12}(t,x)=\sum_{n=0}^{\infty} b_n^{-}(t)r_n(x),$$

with time dependent expansion coefficients $a_n^{\pm}(t)$ and $b_n^{\pm}(t)$. Substitution of Eq. (64) into the coupled partial differential equations (58) and multiplication from left with $l_m(x)$ together with integration over x results in

$$\frac{\partial}{\partial t}a_n^{+}(t)=-n a_n^{+}(t)-\frac{x_0}{2}\sqrt{n}a_{n-1}^{-}(t),$$

$$\frac{\partial}{\partial t}a_n^{-}(t)=-n a_n^{-}(t)-\frac{x_0}{2}\sqrt{n}a_{n-1}^{+}(t)-\tilde{c}b_n^{-}(t),$$

$$\frac{\partial}{\partial t}b_n^{+}(t)=-n b_n^{+}(t)+\tilde{d}\sqrt{n}b_{n-1}^{-}(t)+\tilde{d}\sqrt{n+1}b_{n+1}^{-}(t) -\tilde{d}(x^*(t)-x_0/2)b_n^{-}(t), \tag{65}$$

$$\frac{\partial}{\partial t}b_n^{-}(t)=-n b_n^{-}(t)-\tilde{d}\sqrt{n}b_{n-1}^{+}(t)-\tilde{d}\sqrt{n+1}b_{n+1}^{+}(t) +\tilde{d}(x^*(t)-x_0/2)b_n^{+}(t)+\frac{\tilde{c}}{4}a_n^{-}(t).$$

In deriving this infinite set of linear first-order differential equations for the expansion coefficients we have used the biorthogonality of the basis functions. Note that Eq. (65) we are now confronted with *time-dependent* coefficients due to the time-dependent crossing point $x^*(t)$ [cf. Eq. (60)]. Thus, in the further analysis we cannot simply rely on the standard methods of linear algebra with its fast and well-elaborated numerical algorithms. Instead, we must directly integrate our set of Eqs. (65) numerically. This clearly requires a much larger computational effort as compared to the undriven case!

The sparse linear system (65) has a block tridiagonal structure, where the blocks are 4×4 matrices, corresponding to the four coefficients $a_n^{\pm}, b_n^{\pm}$ for a given n. Note that since $\int_{-\infty}^{\infty}r_n(x)dx=0$ for $n\neq 0$ and $\int_{-\infty}^{\infty}r_0(x)dx=(2\pi)^{1/4}$ it follows from Eqs. (33), (64), and (57) that $P_{11}(t)=\frac{1}{2}(2\pi)^{1/4}[a_0^{+}(t)+a_0^{-}(t)]$ and $P_{22}(t)=\frac{1}{2}(2\pi)^{1/4}[a_0^{+}(t)-a_0^{-}(t)]$. Moreover, from Eq. (65) it follows that $a_0^{+}(t)=\mathrm{const}=a_0^{+}$ is a time-independent constant. The value of this constant as well as the *initial* value of $a_0^{-}(t)$ can be fixed by the initial distribution of electronic populations. Assuming $P_{11}(0)=1$ $[P_{22}(0)=0]$ in the following we get $a_0^{+}(t)=a_0^{-}(0)=1/(2\pi)^{1/4}$. Then, the probability distribution on the surface V_1 reads

$$P_{11}(t)=\tfrac{1}{2}[1+(2\pi)^{1/4}a_0^{-}(t)]. \tag{66}$$

The expansion coefficient $a_0^{-}(t)$ is obtained by integrating Eq. (65) numerically. The rest of initial values $a_n^{+}(0)=a_n^{-}(0)$ is determined from the expansion of the initial distribution $\rho_{11}(x,0)$ over the set $\{r_n(x)\}$. Moreover, $b_n^{\pm}(0)=0$. Note that $P_{11}(t)$, analytically given by Eq. (34) with Eq. (49), and numerically given in Eq. (66) via Eq. (65), is the key quantity in the discussion of driven ET dynamics.

VI. NUMERICAL RESULTS AND DISCUSSION

In this section we shall present our numerical results concerning the Zusman model of electron transfer with external driving. We shall discuss some general features and point out new effects induced by the time dependent fields. Moreover, we compare our novel analytical approximate results versus numerically precise ones.

To evaluate the probability densities $\rho_{ij}(x,t)$ we solve the system of $4\times n$ first order differential equations (65) by using a Runge–Kutta–Merson propagation scheme. Our numerical calculations have shown that usually a set of $n\approx 300$ basis functions is enough to ensure convergence of the results. As initial preparation it is convenient to choose a Gaussian wave packet placed on the donor surface $V_1(x)$, i.e.,

$$\rho_{11}(x,0)=\frac{1}{b_\sigma\sqrt{2\pi}}\exp\left(-\frac{(x-x_\mathrm{I})^2}{2b_\sigma^2}\right), \tag{67}$$

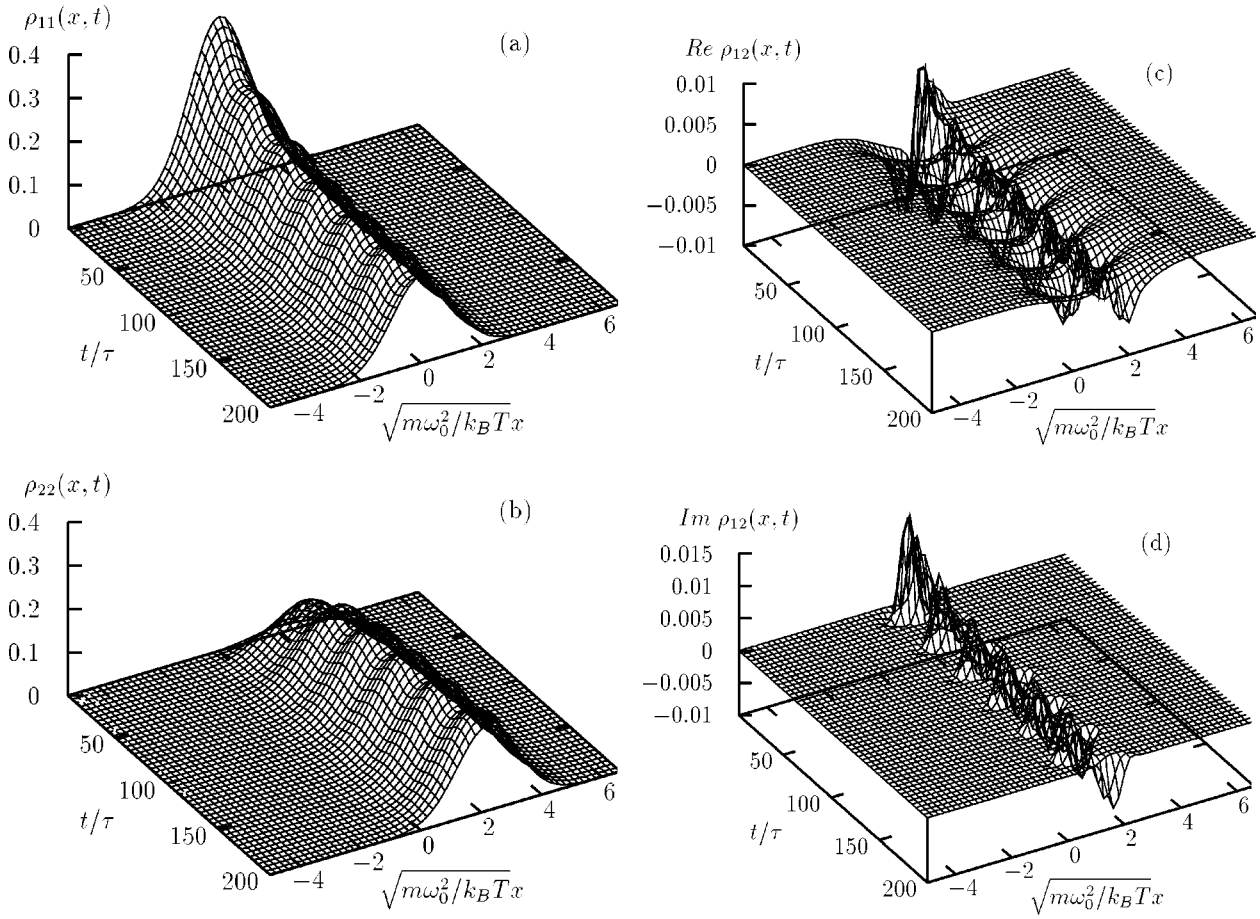

FIG. 3. Dynamics of the reduced density matrix distribution $\rho_{ij}(x,t)$ according to the Zusman equations (15). The calculations for a symmetric system with a vanishing energy gap ($\epsilon_0=0$) between the two surfaces were carried out by the numerical solution of Eqs. (65). The time-dependent field strength $\hat{\epsilon}=250\ \mathrm{cm}^{-1}$ and the frequency $\Omega=1\ \mathrm{cm}^{-1}$ correspond to weak adiabatic driving. The reorganization energy is chosen to be $E_r=500\ \mathrm{cm}^{-1}$ and the temperature is set to $T=300\ \mathrm{K}$. The probability distribution $\rho_{11}(x,t)$ corresponds to the donor potential surface V_{11} while $\rho_{22}(x,t)$ is the probability distribution on the acceptor site.

and $P_{11}(0)=1$. Besides, it is assumed that the Gaussian wave packet has already relaxed to a thermal quasiequilibrium distribution (with electron *fixed* at donor), which explicitly determines the corresponding width b_σ of the distribution and the initial position $x_1=0$. To study the effect of strongly nonequilibrium initial preparations, arbitrary values for b_σ and x_1 can be considered.

In our figures, system and driving parameters are given im units which are commonly used in the ET literature. To explore the influence of time periodic external driving [cf. Eq. (21)] in the Zusman model, we have studied systems characterized by a typical reorganization energy of $E_r=500\ \mathrm{cm}^{-1}$. The energy gap ϵ_0 (bias between the two surfaces) is varied between the normal regime of electron transfer ($|\epsilon_0|<E_r$) and the inverted regime ($|\epsilon_0|>E_r$). The border between these regimes is called the activationless situation where the asymmetry equals the reorganization energy $|\epsilon_0|=E_r$. The calculations are done at room temperature $T=300\ \mathrm{K}$ and the relaxation time τ of the overdamped oscillator is assumed to be 1 ps, if nothing else is stated. Moreover we have used a small coupling strength, $\Delta=10\ \mathrm{cm}^{-1}$, which is two orders of magnitude smaller than the reorganization energy E_r. This parameter choice is quite reasonable for the description of many characteristic nonadiabatic ET reactions.

A. Low-frequency driving

Our considerations start with symmetric systems without bias, $\epsilon_0=0$, i.e., the static system in the absence of driving is in the normal regime. First, we wish to illustrate our numerical procedure with Fig. 3 where we have presented the reduced density matrix distribution $\rho_{ij}(x,t)$. Here, the chosen driving frequency $\Omega=1\ \mathrm{cm}^{-1}$ and driving amplitude $\hat{\epsilon}=250\ \mathrm{cm}^{-1}$ are relatively small compared to the reorganization energy of $E_r=500\ \mathrm{cm}^{-1}$. As a consequence of this very slowly varying driving field the overall effect is an ''adiabatic'' periodic modulation of the energy gap between the two potential wells around the mean value $\epsilon_0=0$. Thus, one can observe an exponential decay of the initial population distributions $\rho_{11}(x,t)$ with superimposed small driving-induced oscillations. Correspondingly, the distribution $\rho_{22}(x,t)$ on the second potential surface $V_2(x)$ depicts an increase of the population. On the slow time scale of the driving the oscillations are best explained within a quasistatic description.

Since the spatial distribution of the reaction coordinate

bears no relevant information for the ET reaction dynamics, we shall concentrate in the subsequent figures on the integrated donor population dynamics $P_{11}(t)$ on the surface $V_{11}(x)$ [cf. Eqs. (33) and (34)]. Moreover, we compare our numerical findings (66) with the analytical predictions given in Eqs. (34) and (49). Here we shall however distinguish between two different approximations for the relaxation rates appearing in Eq. (34). The curves labeled with Γ in our figures correspond to calculations with the full rate constant $\Gamma = k^+ + k^-$ which is composed of the consecutive step forward and backward rates $k^\pm$ in Eq. (49). For comparison, we plotted also calculations with the nonadiabatic rate constant $\Gamma_{\mathrm{NA}} \equiv k^+_{\mathrm{NA}} + k^-_{\mathrm{NA}}$, consisting of the nonadiabatic forward and backward rates $k^\pm_{\mathrm{NA}}$ (50). These latter calculations are labeled with Γ_{NA}.

Figure 4 depicts the numerical results for an intermediate driving frequency $\Omega = 10\,\mathrm{cm}^{-1}$ vs corresponding analytical results. The static energy bias assumes values in the normal ET regime between $\epsilon_0 = 0$ and $\epsilon_0 = 375\,\mathrm{cm}^{-1}$. As expected, we observe a single exponential decay towards a bias-dependent asymptotic long-time limit P_∞. Superimposed on this decay one can still detect some small driving induced oscillations. However, on a long time scale these oscillations are only of secondary importance for the characterization of the ET reaction and they increasingly vanish upon further increasing Ω.

From the good agreement of the numerical findings with the analytic results one can conclude that in Fig. 4 the transfer takes place in the nonadiabatic regime. This is because the dynamics can already be well described with the nonadiabatic rate Γ_{NA} (dashed–dotted line). However, for this low-to-moderate-frequency driving, a closer inspection might indicate that it is slightly more correct to use the full consecutive step rate constant Γ, because, in this case the system is still influenced by the diffusive processes described by the rates $k^\pm_D$ in Eq. (49). The discussion in the next subsection will show that for strong high-frequency driving these diffusion effects are negligible and the reaction becomes even more nonadiabatic.

B. High-frequency driving

In Fig. 5 we consider again a symmetric situation, $\epsilon_0 = 0$, but now the driving field parameters $\hat{\epsilon} = 1400\,\mathrm{cm}^{-1}$ and $\Omega = 500\,\mathrm{cm}^{-1}$ correspond to a strong high-frequency field. The comparison between the exact numerical results (66) (solid line) and the analytical high-frequency results (34) (dashed line Γ, and dashed–dotted line Γ_{NA}) exhibits good agreement for the undriven ($\hat{\epsilon} = 0$) as well as for the driven dynamics. We observe in both cases a single exponential decay of the initial population, without observable oscillations towards the equilibrium donor population $P_\infty = 0.5$. However, for strong high-frequency fields it seems that the dynamics is better described by the nonadiabatic rate Γ_{NA} since this curve *perfectly* matches the numerical results (the two curves are indistinguishable).

1. Consecutive step rate vs nonadiabatic Golden Rule rate

In Fig. 6 we deal with a more complicated situation with finite bias where it is necessary to carefully choose the correct transfer rate in order to correctly describe the *driven* dynamics. Figure 6 depicts results for two biased systems with $\epsilon_0 = 500\,\mathrm{cm}^{-1}$ and $\epsilon_0 = 800\,\mathrm{cm}^{-1}$. In the case without time-dependent driving this corresponds to the activationless situation and to the inverted regime of ET, respectively. Note that in the activationless case ($\epsilon_0 = 500\,\mathrm{cm}^{-1}$) and in the absence of driving ($\hat{\epsilon} = 0$) the analytical result Γ still agrees with the numerics. The nonadiabatic decay rate Γ_{NA} is a slightly larger [see also Fig. 7(a)], but the agreement is satisfactory. The long-time limit P_∞ is independent of the employed rate concept, i.e., Γ vs Γ_{NA}; it is always reproduced correctly.

However, if we now turn to the driven dynamics we can observe something astonishing: the analytical description with the consecutive step rate constant Γ breaks down in this limit of strong high-frequency driving (see dashed lines). Note, that the driving amplitude $\hat{\epsilon} = 1400\,\mathrm{cm}^{-1}$ is almost three times the reorganization energy and we are in the activationless or inverted regime, respectively. However, we find that the ordinary nonadiabatic rate constant $\Gamma_{\mathrm{NA}} = k^+_{\mathrm{NA}} + k^-_{\mathrm{NA}}$ excellently agrees with the numerics. The two curves match each other within line thickness. This is surprising since $k^\pm_{\mathrm{NA}}$ in Eq. (50) is nothing else but the lowest order Golden Rule result in Δ, without contributions from diffusion. Thus, together with the findings in Fig. 4 and Fig. 5 we see the trend that the consecutive step mechanism with the rate Γ (49) is well suited to describe the undriven or weakly driven dynamics. In contrast, the strongly driven dynamics is rather well described by the nonadiabatic Golden Rule result Γ_{NA} in (50). This finding will be confirmed with the next figure.

Figure 7 depicts the different rate constants Γ_{NA} and Γ vs the energy gap ϵ_0 between the two potential surfaces. The case without driving [Fig. 7(a)] as well as the situation with fast strong driving [Fig. 7(b)] are examined. The parameters are the same as in Fig. 6. For comparison also the long-time rates extracted from the full numerical calculations are depicted by the triangles. In Fig. 7(a) it becomes obvious that in absence of driving the numerical results agree best with the consecutive step mechanism that relates to the full rate constant Γ (dashed line). However, the differences with the nonadiabatic rate Γ_{NA} (solid line) are small within the normal, activationless, and inverted ET regimes. With external driving switched on the situation changes [cf. Fig. 7(b)] and Γ_{NA} (dashed line) becomes more appropriate to describe the dynamics. In contrast, the consecutive step rate Γ (dashed line) predicts a too slow decay. The differences with the numerical results become most pronounced in the inverted ET regime.

The reason for this behavior depicted with Fig. 7 is that the diffusion on the diabatic surfaces also experiences an *indirect* influence of the external field via the electronic degree of freedom. Thus, due to an energy flow from the external field this diffusion can be strongly accelerated; it then ceases to act as a limiting factor for the ET reaction. This

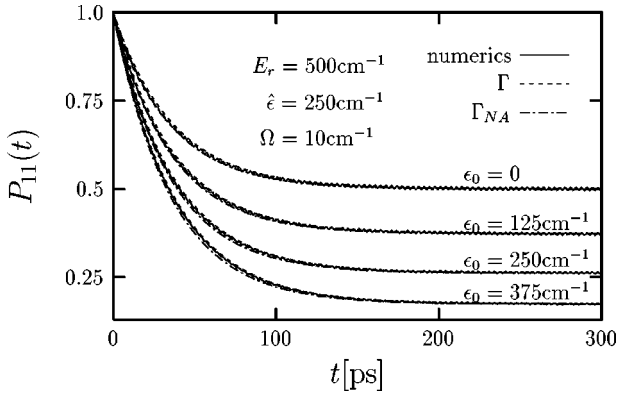

FIG. 4. Time-dependence of the integrated donor population $P_{11}(t)$ on surface $V_{11}(x)$ for moderate driving strength and intermediate driving frequency. For different bias energies ϵ_0 in the normal regime a single exponential decay with superimposed, driving induced oscillations towards the asymptotic long-time limit P_∞ is observed. Besides the exact numerical results (solid line) of Eq. (66) also the analytical predictions of Eq. (34) are depicted. For the full rate constant we used the consecutive step rate $\Gamma = k^+ + k^-$ [dashed line, cf. Eq. (49)] and the ordinary nonadiabatic rate $\Gamma_{\text{NA}} = k^+_{\text{NA}} + k^-_{\text{NA}}$ [dashed-dotted line, cf. Eq. (50)]. Here and in the following figures the temperature is chosen to be $T = 300$ K and the relaxation time of the harmonic oscillator is set to $\tau = 1$ ps. The remaining parameters are given in the figure.

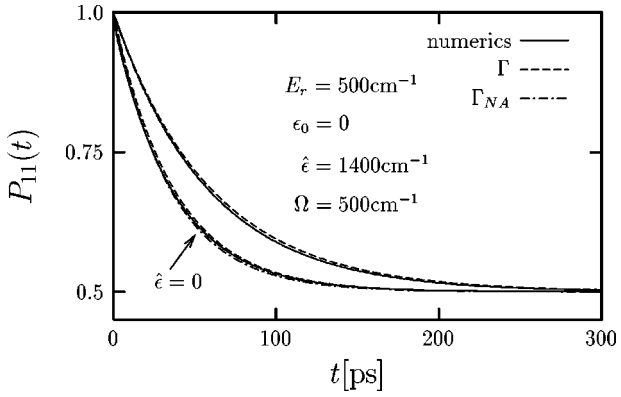

FIG. 5. Numerical and analytical results (cf. Fig. 4) for the dynamics of the integrated donor population $P_{11}(t)$. The ET system is assumed to be symmetric ($\epsilon_0 = 0$) and driven by a strong high-frequency field. The analytical curve obtained by use of the nonadiabatic rate constant (Γ_{NA}, dashed-dotted line) coincides with the numerical findings (solid line). The curve calculated with the consecutive step rate (Γ, dashed line) predicts a slightly slower decay. For comparison also the case without driving ($\hat{\epsilon} = 0$) is depicted. Here, both analytical curves (Γ and Γ_{NA}) provide satisfactory approximations to the exact numerical result.

serves as the explanation why the studied ET reaction becomes increasingly nonadiabatic when strong, fast oscillating fields are applied. Unfortunately, the invoked approximations in deriving Eq. (49) do not respect the mentioned scenario. An improvement would be to take into account also the external field influence on the diffusion, resulting in rates $k_D^{\pm}$ that would depend on the driving field parameters. We leave this interesting issue for a future study.

At this point is is also necessary to comment on the agreement between the numerical results and the analytical results. Actually, just a comparison of the single-exponential, analytical transfer rates (Γ_{NA} or Γ) with numerically extracted long-time decay rates does not provide information on how well the analytic description really describes the full *dynamics* of $P_{11}(t)$. Especially, in the activationless and inverted regime the dynamics has usually to be approximated by a multiexponential decay. In our treatment we disregarded such effects that occur usually on a short initial time scale. However, our numerical studies have shown that for *strong high-frequency driving* the time evolution of $P_{11}(t)$ can very well be described by a *single exponential decay* with the nonadiabatic transfer rate Γ_{NA} (cf. Figs. 5 and 6). This holds true even in the activationless and inverted ET regimes where in the case of zero or weak driving the single-exponential consecutive step approximation already breaks down (not shown).

2. Driving induced inversion of populations

A further appealing feature of external time-dependent driving in the Zusman model is the effect of driving induced inversion of the asymptotic populations, as illustrated with Fig. 6. While in the static, activationless case ($\hat{\epsilon} = 0$, $\epsilon_0 = 500\,\text{cm}^{-1}$) the long time limit P_∞ of the donor population is nearly zero it becomes larger than 1/2 in the driven case for the particular choice of the external field parameters. We thus find more population on the donor surface V_1 than on the acceptor surface V_2 even though the energetic minimum of V_1 is situated $\epsilon_0 = 500\,\text{cm}^{-1}$ above the minimum of V_2!

This effect, already known from the driven spin-boson model,[13,14,18] can also be detected in Fig. 8. Here, the long time value P_∞ (36) of $P_{11}(t)$ is plotted vs the energy bias ϵ_0 for different values of the applied driving strength $\hat{\epsilon}$. The driving frequency $\Omega = 500\,\text{cm}^{-1}$ is held fixed. Inversion of populations, i.e., $P_\infty > 1/2$ for positive bias ϵ_0, can be observed for a strong field amplitude $\hat{\epsilon} = 1400\,\text{cm}^{-1}$ and for a small to moderate bias ϵ_0. The explanation of this phenomenon is similar to that used for the driven spin-boson model.[13,14,18] For a relatively weak resonant field ($\hat{\epsilon} = 500\,\text{cm}^{-1}$) the asymptotic long time limit shows a strictly

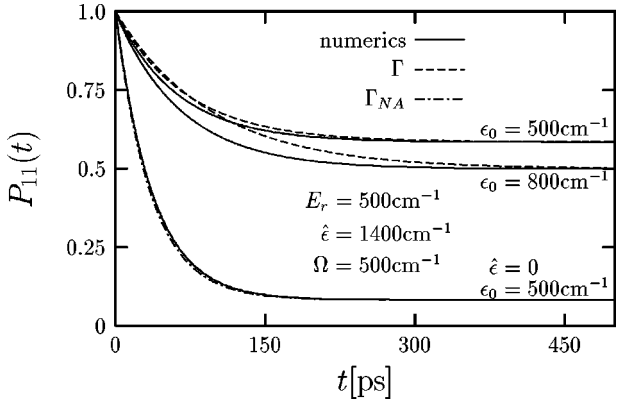

FIG. 6. The figure shows a comparison between the predictions of the exact numerical equation (66) for the donor population $P_{11}(t)$ (solid line) and the analytical approximation (34) with the rate constants Γ and Γ_{NA}, respectively. An activationless situation ($\epsilon_0 = 500\,\text{cm}^{-1}$) and an inverted situation ($\epsilon_0 = 800\,\text{cm}^{-1}$) are considered. The driving field parameters are the same as in Fig. 5. Note that the analytic results with the consecutive rate constant Γ (dashed line) are incorrect while the curve with Γ_{NA} (dashed-dotted line) matches the numerical results exactly. However, the activationless case without driving ($\hat{\epsilon} = 0$, $\epsilon_0 = 500\,\text{cm}^{-1}$) is best described by the curve with Γ.

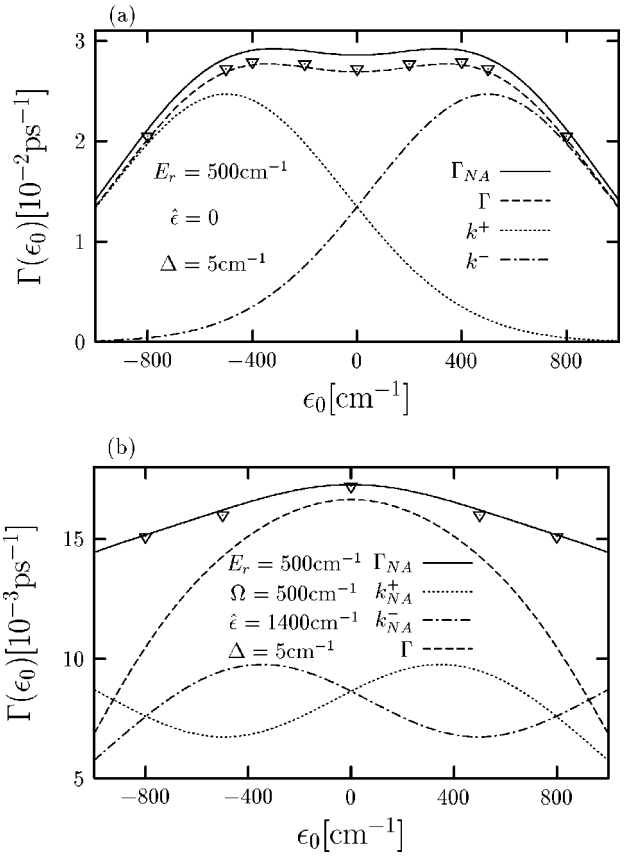

FIG. 7. Dependence of the full ET rate constants $\Gamma = k^+ + k^-$ (dashed line) and $\Gamma_{\mathrm{NA}} = k^+_{\mathrm{NA}} + k^-_{\mathrm{NA}}$ (solid line) on the energy gap ϵ_0 between the two surfaces. For the sake of clarity also the corresponding forward and backward rates $k^{\pm}$ in Eq. (49) (a) or $k^{\pm}_{\mathrm{NA}}$ in Eq. (50) (b) are depicted. Numerically calculated long-time rate constants are indicated by triangles. (a) depicts results for a system without driving. Here, the long-time ET dynamics obeys a consecutive step mechanism (dashed line, Γ). In (b) the strongly driven situation is examined, with the same field parameters as in Figs. 5 and 6. Contrary to (a) now a strict nonadiabatic (solid line, Γ_{NA}) reaction dynamics takes place.

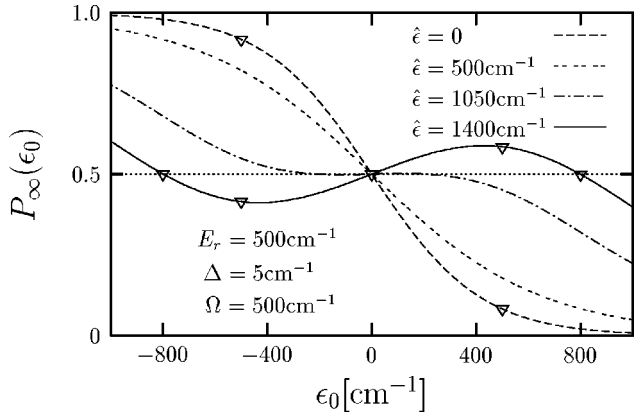

FIG. 8. Driving induced inversion of populations: Plotted is the long time limit $P_{11}(t\to\infty) = P_\infty$ vs the bias ϵ_0 for different values of the applied driving strength $\hat{\epsilon}$. For strong high-frequency driving ($\hat{\epsilon} = 1400\,\mathrm{cm}^{-1}$, solid line) the time-averaged asymptotic equilibrium value P_∞ of the donor population $P_{11}(t)$ becomes larger than 1/2 even though a positive energy gap ϵ_0 is assumed. For comparison corresponding numerical results are indicated by triangles. Likewise for negative ϵ_0 we find the corresponding inversion with $P_\infty < 1/2$.

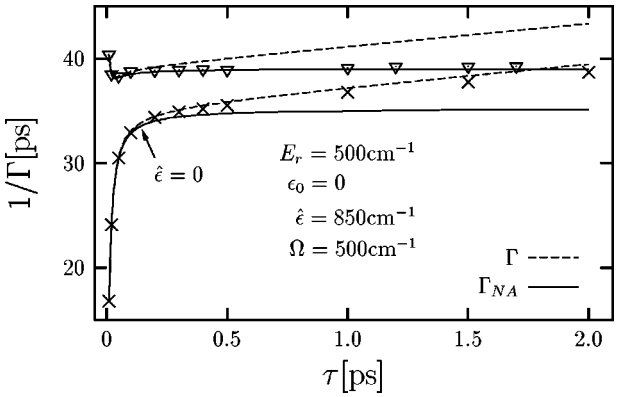

FIG. 9. The reciprocal of the consecutive step transfer rate $\Gamma = k^+ + k^-$ (dashed line) and the nonadiabatic Golden Rule transfer rate $\Gamma_{\mathrm{NA}} = k^+_{\mathrm{NA}} + k^-_{\mathrm{NA}}$ (solid line) as a function of the solvent relaxation time τ. A symmetric system with $\epsilon_0 = 0$ and a high-frequency driving is assumed (the parameters are listed in the figure). Moreover, a comparison with the undriven case ($\hat{\epsilon} = 0$) is depicted. Corresponding results extracted from numerical calculations are indicated by triangles and crosses, respectively.

monotonic behavior with decreasing P_∞ for strongly biased systems, similar to the static case ($\hat{\epsilon} = 0$), which is also depicted. Finally, with $\hat{\epsilon} = 1050\,\mathrm{cm}^{-1}$ the driving amplitude is chosen in such a way, to result in a bias independent P_∞ for small bias. Note that also in this figure numerical results are indicated by the triangles. Moreover, we want to mention that our numerical studies prove that the driven long-time limit P_∞ is always correctly given by the analytical formula (36). Thus, P_∞ depends only on the long-time rates, and differences of the exact numerical results and the analytics in the time-dependent dynamics of $P_{11}(t)$ do not become relevant at asymptotic times. We also recall again that with time-dependent driving P_∞ cannot be determined from the detailed balance condition.

3. Driving-induced crossover to nonadiabatic transfer

Figures 9 and 10 depict the analytical dependence of the total consecutive step rate $\Gamma = k^+ + k^-$ and the total nonadia-

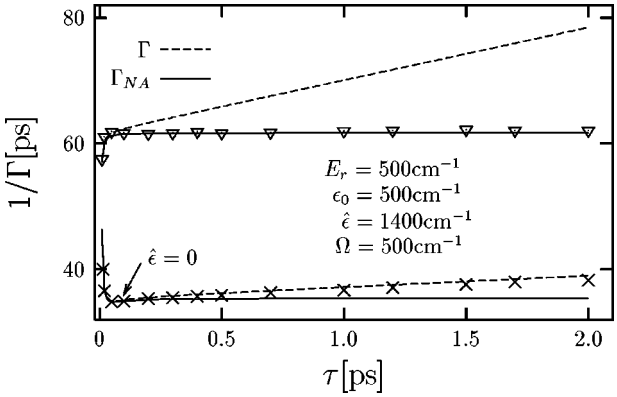

FIG. 10. Dependence of the reciprocal transfer rates $\Gamma = k^+ + k^-$ (dashed line) and $\Gamma_{\mathrm{NA}} = k^+_{\mathrm{NA}} + k^-_{\mathrm{NA}}$ (solid line) on the solvent relaxation time τ in the high-frequency driving regime. Here, the energy gap $\epsilon_0 = 500\,\mathrm{cm}^{-1}$ corresponds to an activationless situation. The comparison with the undriven case ($\hat{\epsilon} = 0$) is depicted also. Corresponding numerical results are indicated by triangles and crosses, respectively.

batic rate $\Gamma_{NA}=k_{NA}^{+}+k_{NA}^{-}$ vs the relaxation time τ of the harmonic oscillator. The corresponding system and driving parameters are listed in the figures.

First, we want to discuss the undriven case, marked in both figures with $\hat{\epsilon}=0$. Clearly, the Γ^{-1} vs τ curve can be separated into two different regions. For large τ the reciprocal of the ET rate is proportional to τ which is an indicator for the solvent-controlled adiabatic limit (dashed line). This type of behavior is robust against the variation of the energy gap ϵ_0 (cf. Figs. 9 and 10) and was predicted previously.[5,33] It agrees well with our numerical findings indicated by the crosses. The nonadiabatic rate Γ_{NA} (solid line) fails in this regime. However, the behavior for very small τ depends qualitatively on the bias between the two surfaces. For the symmetric system in Fig. 9 the transfer rate Γ rapidly increases with decreasing τ, while for the activationless situation in Fig. 10 an opposite behavior is observed. In this regime the consecutive step rate Γ and the nonadiabatic rate Γ_{NA} always become the same, meaning nonadiabatic reaction dynamics. In the transition region between ''large'' and ''small'' relaxation times τ the situation is not completely clear. Here, the rate depends only weakly on τ which is usually named the ''normal'' nonadiabatic behavior.

If we now apply a strong high-frequency driving we observe the same striking effect as already encountered in the previous figures. Our numerical results in Figs. 9 and 10 (indicated by the triangles) make it evident that for large τ the time-dependent external field promotes the transition from the adiabatic to the nonadiabatic regime of ET. While in the undriven case the reciprocal rate was depending on $\tau, \Gamma^{-1}\sim\tau$ (adiabatic regime), the rate with driving becomes increasingly independent of the relaxation time. This is a hallmark of the nonadiabatic reaction regime and consequently the electron transfer has to be described by Γ_{NA} (straight solid line). This important result is independent of whether a symmetric system (Fig. 9) or an activationless system (Fig. 10) is considered as long as the driving strength $\hat{\epsilon}$ and frequency Ω are large enough. For intermediate driving fields the situation is more complicated and neither a strict adiabatic nor a strict nonadiabatic behavior is to be expected (not shown).

Our results represent a prominent manifestation of the *improvement* of the Golden Rule type description of ET processes *due to time-dependent fields*. This result is rather unexpected because the nonadiabatic Golden Rule rate Γ_{NA} corresponds just to the lowest order perturbation theory in the tunneling matrix element Δ.

As a last point of our considerations it is worth mentioning that the above discussions lead us to the conclusion that a field-induced transition in the opposite direction, i.e., *from the nonadiabatic to the adiabatic transfer regime* is barely possible for the present model. Indeed, we were not able to find such a regime numerically, albeit its presence is demonstrated by Eq. (49).

VII. CONCLUDING REMARKS

In this work we have studied the generalized Zusman model of electron transfer in presence of strong driving fields $\mathcal{E}(t)$. It was shown that the original Zusman equations can be generalized to the driven case by simple replacing the static energy bias with the time-dependent one. We have studied these so generalized equations both numerically and analytically. A (in Δ) nonperturbative rate expression (49) has been derived. It generalizes the one given earlier in Ref. 19 to the driven, time-dependent case. Moreover, by doing so, we also generalize the driven nonadiabatic ET theories of Dakhnovskii and Coalson[13] and others[14,17] beyond Golden Rule theory away from fast and strong driving. Testing this rate expression against the precise numerics shows that it works excellently for the *undriven* case and in the *normal* regime of electron transfer. Moreover, this expression still works for the driven case, if the driving frequency is not too high. However, for a ''nonadiabatic,'' high-frequency driving it even fails already *in the normal regime*. Instead, the familiar nonadiabatic rate expression (50) extends drastically its regime of applicability. For sufficiently large solvent autocorrelation times τ it may happen that instead of the linear dependence of the inverse ET rate, $\Gamma^{-1}\propto\tau$, on τ (solvent controlled ET), the transfer rate becomes *independent* of τ, if the driving field is switched on. This result manifests that a strong and fast periodic driving can introduce a crossover from the adiabatic (solvent controlled) to the nonadiabatic ET regime. This is the major finding of this work. In terms of a perturbation theory in the electronic coupling Δ, our results prove that strong and fast periodic driving *improves* the quality of low order perturbation theory in Δ. As a result, its lowest order approximation, i.e., the Golden Rule, becomes sufficient to describe ET dynamics even there, where it was clearly not applicable before, in the absence of driving.

ACKNOWLEDGMENTS

This work has been supported by the Deutsche Forschungsgemeinschaft within the Schwerpunktsprogramm *Zeitabhängige Phänomene und Methoden in Quantensystemen der Physik und Chemie*, HA1517/14-3, and within the Sonderforschungsbereich 486, project A10. We also like to acknowledge helpful discussions with E. Pollak.

APPENDIX: GREEN FUNCTIONS FOR THE HARMONIC POTENTIALS

1. The off-diagonal Green function

For harmonic potential surfaces $V_1(x)$ and $V_2(x)$ the operator (20) becomes similar to that for the Ornstein–Uhlenbeck process with a linear drift coefficient and a constant diffusion coefficient. Therefore, we expect to find an analytic expression for the complex-valued Green function $G(x,t|x',t')$ in Eq. (20). By use of the potentials (5) and the phenomenological relaxation time of the overdamped oscillator $\tau=\gamma/\omega_0^2$, the equation for the Green function reads

$$\frac{\partial}{\partial t}G(x,t|x',t')=\left[D\frac{\partial^2}{\partial x^2}+\frac{1}{\tau}\frac{\partial}{\partial x}(x-x_0/2)-\frac{i}{\hbar}\left(\frac{2E_r}{x_0}(x-x_0/2)+\epsilon_0+\epsilon(t)\right)\right]\times G(x,t'|x',t'), \tag{A1}$$

with the initial condition $G(x,t'|x',t')=\delta(x-x')$ and the boundary conditions $G(\pm\infty,t'|x',t')=0$. Note immediately that the solution of Eq. (A1) can be considered in the form

$$G(x,t|x',t')=G_0(x,t-t'|x')\exp\left[-\frac{i}{\hbar}\zeta(t,t')\right], \quad \text{(A2)}$$

where $G_0(x,t-t'|x')$ is the Green function of a similar static ($\epsilon(t)=0$) and symmetric ($\epsilon_0=0$) problem, and where

$$\zeta(t,t')=\int_{t'}^{t}dt''[\epsilon_0+\epsilon(t'')] \quad \text{(A3)}$$

accounts both for the energy bias ϵ_0 and for the external driving field influence $\epsilon(t)$. While $G_0(x,t-t'|x')$ depends only on the time difference, the driving function $\zeta(t,t')$ explicitly depends on both time arguments and thus also the Green function itself. Obviously, the Green function $G_0(x,t-t'|x')$ satisfies Eq. (A1) with $\epsilon(t)=0$ and $\epsilon_0=0$. Its solution is obtained by making a Fourier transform with respect to x, i.e.,

$$\tilde{G}_0(k,t|x')=\frac{1}{\sqrt{2\pi}}\int_{-\infty}^{+\infty}dx e^{ikx}G_0(x,t|x'). \quad \text{(A4)}$$

The equation for the Fourier transform is given by

$$\frac{\partial}{\partial t}\tilde{G}_0(k,t|x')=\left[-Dk^2-\frac{k}{\tau}\frac{\partial}{\partial k}+\frac{ikx_0}{2\tau}-\frac{2E_r}{\hbar x_0}\frac{\partial}{\partial k}+\frac{i}{\hbar}E_r\right]\times\tilde{G}_0(k,t|x'), \quad \text{(A5)}$$

which is simpler than Eq. (A1) because only first-order derivatives with respect to k occur. The initial condition for the Fourier transform becomes $\tilde{G}_0(k,0|x')=\exp(ikx')/\sqrt{2\pi}$. With the ansatz,

$$\tilde{G}_0(k,t|x')=\frac{1}{\sqrt{2\pi}}\exp[-a(t)k^2-b(t)k-c(t)], \quad \text{(A6)}$$

where the time dependent functions $a(t)$, $b(t)$, and $c(t)$ have to be calculated, one finds after some lengthy algebra and transformation back to the time domain the final result

$$G_0(x,t|x')=\frac{1}{\sqrt{\pi A(t)}}\exp\left[\frac{(B(x',t)-ix)^2}{A(t)}+C(x',t)\right]. \quad \text{(A7)}$$

Here, we have introduced the functions

$$A(t)=2D\tau(1-e^{-2t/\tau}), \quad \text{(A8)}$$

$$B(x',t)=\frac{k_BT\tau}{\hbar}x_0(1-e^{-t/\tau})^2+i\frac{1}{2}x_0(1-e^{-t/\tau})+ix'e^{-t/\tau}, \quad \text{(A9)}$$

$$C(x',t)=\frac{E_rk_BT\tau^2}{\hbar^2}\left(\frac{1}{2}(1-e^{-t/\tau})^2+(1-e^{-t/\tau})-\frac{t}{\tau}\right)+\frac{i2E_r\tau}{\hbar x_0}\left(\frac{1}{2}x_0-x'\right)(1-e^{-t/\tau}). \quad \text{(A10)}$$

As expected, the Green function $G_0(x,t|x')$ obeys for times $t>0$ a Gaussian distribution. Our result for $G_0(x,t|x')$ replaces the incorrect one given in Ref. 20.

2. The diagonal Green functions

The evaluation of the remaining propagators $G_{1,2}(x,t-t'|x')$ in Eq. (27) causes even less problems for harmonic potential surfaces. The process described by the equation,

$$\frac{\partial}{\partial t}G_1(x,t-t'|x')=\left[D\frac{\partial^2}{\partial x^2}+\frac{1}{\tau}\frac{\partial}{\partial x}x\right]G_1(x,t-t'|x'), \quad \text{(A11)}$$

is just the Ornstein–Uhlenbeck process. The corresponding solution is well known and given by[29]

$$G_1(x,t-t'|x')=\frac{1}{\sqrt{2\pi D\tau(1-e^{-2(t-t')/\tau})}}\times\exp\left[\frac{-(x-x'e^{-(t-t')/\tau})^2}{2D\tau(1-e^{-2(t-t')/\tau})}\right]. \quad \text{(A12)}$$

The expression for $G_2(x,t-t'|x')$ is obtained from Eq. (A12) by the substitutions $x\to(x-x_0)$ and $x'\to(x'-x_0)$, respectively.

[1] *Electron Transfer: From Isolated Molecules to Biomolecules*, edited by J. Jortner and M. Bixon, Adv. Chem. Phys. **106** (Part I), **107** (Part II) (1999).
[2] R. A. Marcus, J. Chem. Phys. **24**, 966 (1956); **26**, 867 (1957); Discuss. Faraday Soc. **29**, 21 (1960).
[3] N. S. Hush, J. Chem. Phys. **28**, 962 (1958).
[4] V. G. Levich and R. R. Dogonadze, Dokl. Akad. Nauk SSSR **124**, 123 (1959); [Proc. Acad. Sci. Phys. Chem. Sect. **124**, 9 (1959)].
[5] L. D. Zusman, Chem. Phys. **49**, 295 (1980).
[6] I. V. Alexandrov, Chem. Phys. **51**, 449 (1980).
[7] A. Garg, J. N. Onuchic, and V. Ambegaokar, J. Chem. Phys. **83**, 4491 (1985).
[8] J. Tang, J. Chem. Phys. **104**, 9408 (1996).
[9] T. Fonseca, J. Chem. Phys. **91**, 2869 (1989).
[10] L. D. Zusman and D. N. Beratan, J. Chem. Phys. **105**, 165 (1996).
[11] L. D. Zusman and D. N. Beratan, J. Chem. Phys. **110**, 10468 (1999).
[12] T. Bandyopadhyay, A. Okada, and M. Tachiya, J. Chem. Phys. **110**, 9630 (1999).
[13] (a) Yu. Dakhnovskii and R. D. Coalson, J. Chem. Phys. **103**, 2908 (1995); (b) Yu. Dakhnovskii, D. G. Evans, H. J. Kim, and R. D. Coalson, *ibid.* **103**, 5461 (1995).
[14] I. A. Goychuk, E. G. Petrov, and V. May, Chem. Phys. Lett. **253**, 428 (1996).
[15] I. A. Goychuk, E. G. Petrov, and V. May, J. Chem. Phys. **106**, 4522 (1997); in *Proceedings of the Conference ''Electron and Ion Transfer in Condensed Media,'' ICTP, Trieste, 15–19 July 1996*, edited by A. A. Kornyshev, M. Tosi, and J. Ulstrup (World Scientific, Singapore, 1997), pp. 362–371.
[16] I. A. Goychuk, E. G. Petrov, and V. May, Phys. Rev. E **56**, 1421 (1997).
[17] M. Grifoni, L. Hartmann, and P. Hänggi, Chem. Phys. **217**, 167 (1997).
[18] M. Grifoni and P. Hänggi, Phys. Rep. **304**, 229 (1998).
[19] D. Y. Yang and R. I. Cukier, J. Chem. Phys. **91**, 281 (1989).
[20] D. Y. Yang, J. Stat. Phys. **74**, 631 (1994).
[21] H. Köppel, W. Domcke, and L. S. Cederbaum, Adv. Chem. Phys. **57**, 59 (1984).
[22] A. O. Caldeira and A. J. Leggett, Physica A **121**, 587 (1983).
[23] R. M. Stratt and M. Marconelli, J. Phys. Chem. **100**, 12981 (1996).
[24] M. Marchi, J. N. Gehlen, D. Chandler, and M. Newton, J. Am. Chem. Soc. **115**, 4178 (1993).
[25] W. J. Munro and C. W. Gardiner, Phys. Rev. A **53**, 2633 (1996).
[26] E. Wigner, Phys. Rev. **40**, 749 (1932).
[27] M. Hillery, R. F. O'Connell, M. O. Scully, and E. P. Wigner, Phys. Rep. **106**, 122 (1984).

[28] C. W. Gardiner, *Quantum Noise* (Springer, Berlin, 1991), p. 134.
[29] H. Risken, *The Fokker–Planck Equation* (Springer-Verlag, Berlin, 1984).
[30] H. Risken, H. D. Vollmer, and M. Mörsch, Z. Phys. B: Condens. Matter **40**, 343 (1981).
[31] Z. Wang, J. Tang, and J. R. Norris, J. Chem. Phys. **97**, 7251 (1992).
[32] S. Roy and B. Bagchi, J. Chem. Phys. **100**, 8802 (1994).
[33] J. Tang and J. Norris, J. Chem. Phys. **101**, 5615 (1994).
[34] An improvement of this approximation is expected to result by using the shifted peak points $\{x_n^*\}$ instead [see below Eq. (31)]; this, however, yields rather intractable results. Work to overcome this challenge is presently in progress. In fact, by invoking this ad hoc type of approximation we do neglect the indirect influence of the external time-periodically varying field on the diffusion rates.
[35] M. Morillo and R. I. Cukier, J. Chem. Phys. **89**, 6736 (1988).
[36] J. Tang and S. H. Lin, J. Chem. Phys. **107**, 3485 (1997).
[37] Indeed, proceeding as in Ref. 7 we can obtain this result alternatively from our model [cf. Eqs. (3) and (5)] in the following manner. First, we assume the harmonic reaction coordinate x to be in thermal equilibrium with the bath of $N(N\to\infty)$ harmonic oscillators $\{x_i\}$. Then, one can perform a canonical transformation to a bath of $N+1$ harmonic oscillators which yields a spin-boson model with the effective spectral density $J_{\mathrm{eff}}(\omega)=m\gamma\omega_0^4\omega/[(\omega^2-\omega_0^2)^2+\omega^2\gamma^2]$. For the respective details of the calculation we refer the readers to Garg *et al.* (Ref. 7). Next, we note that in the overdamped limit $\gamma\gg\omega_0$,$J_{\mathrm{eff}}(\omega)$ can be well approximated by $J_{\mathrm{Debye}}(\omega)$, where we utilize $\tau=\gamma/\omega_0^2$ and $E_r=m\omega_0^2x_0^2/2$. Finally, using $J_{\mathrm{Debye}}(\omega)$ in the standard Golden Rule formula of the spin-boson model (see e.g., Refs. 7 and 36) we obtain in the high-temperature limit, $k_BT\gg\hbar/\tau$, our Eq. (50) with $\hat{\epsilon}=0$.
[38] I. S. Gradstein and I. M. Ryzhik, *Table of Integrals, Series, and Products* (Academic, New York, 1965).
[39] A. Starobinets, I. Rips, and E. Pollak, J. Chem. Phys. **104**, 6547 (1996).
[40] H. A. Kramers, Physica (Utrecht) **7**, 284 (1940).
[41] P. Hänggi, P. Talkner, and M. Borcovec, Rev. Mod. Phys. **62**, 251 (1990).
[42] I. Rips and J. Jortner, J. Chem. Phys. **87**, 6513 (1987); **87**, 2090 (1987).